

# A FLEXIBLE METHOD OF ESTIMATING LUMINOSITY FUNCTIONS

BRANDON C. KELLY<sup>1</sup>, XIAOHUI FAN,

Steward Observatory, University of Arizona, 933 N Cherry Ave, Tucson, AZ 85721

AND

MARIANNE VESTERGAARD

Dept. of Physics and Astronomy, Robinson Hall, Tufts University, Medford, MA 02155

*Draft version February 10, 2022*

## ABSTRACT

We describe a Bayesian approach to estimating luminosity functions. We derive the likelihood function and posterior probability distribution for the luminosity function, given the observed data, and we compare the Bayesian approach with maximum-likelihood by simulating sources from a Schechter function. For our simulations confidence intervals derived from bootstrapping the maximum-likelihood estimate can be too narrow, while confidence intervals derived from the Bayesian approach are valid. We develop our statistical approach for a flexible model where the luminosity function is modeled as a mixture of Gaussian functions. Statistical inference is performed using Markov chain Monte Carlo (MCMC) methods, and we describe a Metropolis-Hastings algorithm to perform the MCMC. The MCMC simulates random draws from the probability distribution of the luminosity function parameters, given the data, and we use a simulated data set to show how these random draws may be used to estimate the probability distribution for the luminosity function. In addition, we show how the MCMC output may be used to estimate the probability distribution of any quantities derived from the luminosity function, such as the peak in the space density of quasars. The Bayesian method we develop has the advantage that it is able to place accurate constraints on the luminosity function even beyond the survey detection limits, and that it provides a natural way of estimating the probability distribution of any quantities derived from the luminosity function, including those that rely on information beyond the survey detection limits.

*Subject headings:* galaxies: luminosity function — methods: data analysis — methods: numerical — methods: statistical

## 1. INTRODUCTION

The luminosity function (LF) has been an important tool for understanding the evolution of galaxies and quasars, as it provides a census of the galaxy and quasar populations over cosmic time. Quasar luminosity functions have been estimated for optical surveys (e.g., Fan et al. 2001; Wolf et al. 2003; Croom et al. 2004; Richards et al. 2006; Jiang et al. 2006), X-ray surveys (e.g., Steffen et al. 2003; Ueda et al. 2003; Barger et al. 2005; La Franca et al. 2005), infrared surveys (e.g., Barger et al. 2005; Matute et al. 2006; Babbedge et al. 2006), radio surveys (e.g., Waddington et al. 2001; Willott et al. 2001), and emission lines (Hao et al. 2005). In addition, luminosity functions across different bands have been combined to form an estimate of the bolometric luminosity function (Hopkins et al. 2007). Besides providing an important constraint on models of quasar evolution and supermassive black hole growth (e.g., Wyithe & Loeb 2003; Hopkins et al. 2006a), studies of the LF have found evidence for ‘cosmic downsizing’, where the space density of more luminous quasars peaks at higher redshift. Attempts to map the growth of supermassive black holes start from the local supermassive black hole distribution, and employ the argument of Soltan (1982), using the quasar luminosity function as a constraint on the black hole mass distribution. These studies have found evidence that the highest mass black holes grow first (e.g., Yu & Tremaine 2002; Marconi et al. 2004; Merloni 2004), suggesting that this cosmic downsizing is the result of an anti-hierarchical growth of supermassive black holes.

Similarly, galaxy luminosity functions have been estimated in the optical (e.g., Blanton et al. 2003; Dahlen et al. 2005; Brown et al. 2007; Marchesini et al. 2007), X-ray (e.g., Kim et al. 2006; Ptak et al. 2007), infrared (e.g., Cirasuolo et al. 2007; Huynh et al. 2007), ultraviolet (e.g., Budavári et al. 2005; Paltani et al. 2007), radio (e.g., Lin & Mohr 2007; Mauch & Sadler 2007), for galaxies in clusters (e.g., Popesso et al. 2006; Harsono & de Propris 2007), and for galaxies in voids (Hoyle et al. 2005). The galaxy luminosity function probes several aspects of the galaxy population; namely (a) the evolution of stellar populations and star formation histories (e.g., Faber et al. 2007), (b) the local supermassive black hole mass distribution (e.g., Yu & Tremaine 2002; Marconi et al. 2004) via the Magorrian relationship (Magorrian et al. 1998), (c) the dependence of galaxy properties on environment (e.g., Croton et al. 2005; Lauer et al. 2007), and (d) places constraints on models of structure formation and galaxy evolution (e.g., Bower et al. 2006; Finlator et al. 2006; Marchesini & van Dokkum 2007).

Given the importance of the luminosity function as an observational constraint on models of quasar and galaxy evolution, it is essential that a statistically accurate approach be employed when estimating these quantities. However,

<sup>1</sup> bkelly@as.arizona.edu

the existence of complicated selection functions hinders this, and, as a result, a variety of methods have been used to accurately account for the selection function when estimating the LF. These include various binning methods (e.g., Schmidt 1968; Avni & Bahcall 1980; Page & Carrera 2000), maximum-likelihood fitting (e.g., Marshall et al. 1983; Fan et al. 2001), and a powerful semi-parametric approach (Schafer 2007). In addition, there have been a variety of methods proposed for estimating the cumulative distribution function of the LF (e.g., Lynden-Bell 1971; Efron & Petrosian 1992; Maloney & Petrosian 1999).

Each of these statistical methods has advantages and disadvantages. Statistical inference based on the binning procedures cannot be extended beyond the support of the selection function, and the cumulative distribution function methods typically assume that luminosity and redshift are statistically independent. Furthermore, one is faced with the arbitrary choice of bin size. The maximum-likelihood approach typically assumes a restrictive and somewhat *ad hoc* parametric form, and has not been used to give an estimate of the LF normalization; instead, for example, the LF normalization is often chosen to make the expected number of sources detected in one's survey equal to the actual number of sources detected. In addition, confidence intervals based on the errors derived from the various procedures are typically derived by assuming that the uncertainties on the LF parameters have a Gaussian distribution. While this is valid as the sample size approaches infinity, it is not necessarily a good approximation for finite sample sizes. This is particularly problematic if one is employing the best fit results to extrapolating the luminosity function beyond the bounds of the selection function. It is unclear if the probability distribution of the uncertainty in the estimated luminosity function below the flux limit is even asymptotically normal.

Motivated by these issues, we have developed a Bayesian method for estimating the luminosity function. We derive the likelihood function of the LF by relating the observed data to the true LF, assuming some parametric form, and derive the posterior probability distribution of the LF parameters, given the observed data. While the likelihood function and posterior are valid for any parametric form, we focus on a flexible parametric model where the LF is modeled as a weighted sum of Gaussian functions. This is a type of 'non-parametric' approach, where the basic idea is that the individual Gaussian functions do not have any physical meaning, but that given enough Gaussian functions one can obtain a suitably accurate approximation to the true LF; a similar approach has been taken by Blanton et al. (2003) for estimating galaxy LFs, and by Kelly (2007) within the context of linear regression with measurement error. Modeling the LF as a mixture of Gaussian functions avoids the problem of choosing a particular parametric form, especially in the absence of any guidance from astrophysical theory. The mixture of Gaussians model has been studied from a Bayesian perspective by numerous authors (e.g., Roeder & Wasserman 1997; Jasra et al. 2005; Dellaportas & Papageorgiou 2006). In addition, we describe a Markov chain Monte Carlo (MCMC) algorithm for obtaining random draws from the posterior distribution. These random draws allow one to estimate the posterior distribution for the LF, as well as any quantities derived from it. The MCMC method therefore allows a straightforward method of calculating uncertainties on any quantity derived from the LF, such as the redshift where the space density of quasars or galaxies peaks; this has proven to be a challenge for other statistical methods developed for LF estimation. Because the Bayesian approach is valid for any sample size, one is therefore able to place reliable constraints on the LF and related quantities even below the survey flux limits.

Because of the diversity and mathematical complexity of some parts of this paper, we summarize the main results here. We do this so that the reader who is only interested in specific aspects of this paper can conveniently consult the sections of interest.

- In § 2 we derive the general form of the likelihood function for luminosity function estimation. We show that the commonly used likelihood function based on the Poisson distribution is incorrect, and that the correct form of the likelihood function is derived from the binomial distribution. However, because the Poisson distribution is the limit of the binomial distribution as the probability of including a source in a survey approaches zero, the maximum-likelihood estimates derived from the two distributions give nearly identical results so long as a survey's detection probability is small. The reader who is interested in using the correct form of the likelihood function of the LF should consult this section.
- In § 3 we describe a Bayesian approach to luminosity function estimation. We build on the likelihood function derived in § 2 to derive the probability distribution of the luminosity function, given the observed data (i.e., the posterior distribution). We use a simple example based on a Schechter function to illustrate the Bayesian approach, and compare it with the maximum-likelihood approach. For this example, we find that confidence intervals derived from the posterior distribution are valid, while confidence intervals derived from bootstrapping the maximum-likelihood estimate can be too small. The reader who is interested in a Bayesian approach to luminosity function estimation, and how it compares with maximum-likelihood, should consult this section.
- In § 4 we develop a mixture of Gaussian functions model for the luminosity function, deriving the likelihood function and posterior distribution for the model. Under this model, the LF is modeled as a weighted sum of Gaussian functions. This model has the advantage that given a suitably large enough number of Gaussian functions, it is flexible enough to give an accurate estimate of any smooth and continuous LF. This allows the model to adapt to the true LF, thus minimizing the bias that can result when assuming a parametric form of the LF. This is particularly useful when extrapolating beyond the flux limits of a survey, where bias caused by parametric misspecification can be a significant concern. The reader who are interested in employing the mixture of Gaussian functions model should consult this section.

- Because of the large number of parameters often associated with luminosity function estimation, Bayesian inference is most easily performed by obtaining random draws of the LF from the posterior distribution. In § 5 we describe the Metropolis-Hastings algorithm (MHA) for obtaining random draws of the LF from the posterior distribution. As an example, we describe a MHA for obtaining random draws of the parameters for a Schechter function from the posterior distribution. Then, we describe a more complex MHA for obtaining random draws of the parameters for the mixture of Gaussian functions model. The reader who is interested in the computational aspects of ‘fitting’ the mixture of Gaussian functions model, or who is interested in the computational aspects of Bayesian inference for the LF, should consult this section. A computer routine for performing the Metropolis-Hastings algorithm for the mixture of Gaussian functions model is available on request from B. Kelly.
- In § 6 we use simulation to illustrate the effectiveness of our Bayesian Gaussian mixture model for luminosity function estimation. We construct a simulated data set similar to the Sloan Digital Sky Survey DR3 Quasar Catalog (Schneider et al. 2005). We then use our mixture of Gaussian functions model to recover the true LF and show that our mixture model is able to place reliable constraints on the LF. We also illustrate how to use the MHA output to constrain any quantity derived from the LF, and how to use the MHA output to assess the quality of the fit. The reader who is interested in assessing the effectiveness of our statistical approach, or who is interested in using the MHA output for statistical inference on the LF, should consult this section.

We adopt a cosmology based on the the WMAP best-fit parameters ( $h = 0.71, \Omega_m = 0.27, \Omega_\Lambda = 0.73$ , Spergel et al. 2003)

## 2. THE LIKELIHOOD FUNCTION

### 2.1. Notation

We use the common statistical notation that an estimate of a quantity is denoted by placing a ‘hat’ above it; e.g.,  $\hat{\theta}$  is an estimate of the true value of the parameter  $\theta$ . The parameter  $\theta$  may be scalar or multivalued. We denote a normal density<sup>1</sup> (i.e., a Gaussian distribution) with mean  $\mu$  and variance  $\sigma^2$  as  $N(\mu, \sigma^2)$ , and we denote as  $N_p(\mu, \Sigma)$  a multivariate normal density with  $p$ -element mean vector  $\mu$  and  $p \times p$  covariance matrix  $\Sigma$ . If we want to explicitly identify the argument of the Gaussian function, we use the notation  $N(x|\mu, \sigma^2)$ , which should be understood to be a Gaussian with mean  $\mu$  and variance  $\sigma^2$  as a function of  $x$ . We will often use the common statistical notation where “ $\sim$ ” means “is drawn from” or “is distributed as”. This should not be confused with the common usage of implying “similar to”. For example,  $x \sim N(\mu, \sigma^2)$  states that  $x$  is drawn from a normal density with mean  $\mu$  and variance  $\sigma^2$ , whereas  $x \sim 1$  states that the value of  $x$  is similar to one.

In this work, the maximum-likelihood estimate of the luminosity function refers to an estimate of the LF obtained by maximizing the likelihood function of the unbinned data. Therefore, the maximum-likelihood estimate does not refer to an estimate obtained by maximizing the likelihood function of binned data, such as fitting the results obtained from the  $1/V_a$  technique.

### 2.2. Derivation of the Luminosity Function Likelihood

The luminosity function, denoted as  $\phi(L, z)dL$ , is the number of sources per comoving volume  $V(z)$  with luminosities in the range  $L, L + dL$ . The luminosity function is related to the probability density of  $(L, z)$  by

$$p(L, z) = \frac{1}{N} \phi(L, z) \frac{dV}{dz}, \quad (1)$$

where  $N$  is the total number of sources in the observable universe, and is given by the integral of  $\phi$  over  $L$  and  $V(z)$ . Note that  $p(L, z)dLdz$  is the probability of finding a source in the range  $L, L + dL$  and  $z, z + dz$ . Equation (1) separates the LF into its shape, given by  $p(L, z)$ , and its normalization, given by  $N$ . Once we have an estimate of  $p(L, z)$ , we can easily convert this to an estimate of  $\phi(L, z)$  using Equation (1). In general, it is easier to work with the probability distribution of  $L$  and  $z$ , instead of directly with the LF, because  $p(L, z)$  is more directly related to the likelihood function.

If we assume a parametric form for  $\phi(L, z)$ , with parameters  $\theta$ , we can derive the likelihood function for the observed data. The likelihood function is the probability of observing one’s data, given the assumed model. The presence of flux limits and various other selection effects can make this difficult, as the observed data likelihood function is not simply given by Equation (1). In this case, the set of luminosities and redshifts observed by a survey gives a biased estimate of the true underlying distribution, since only those sources with  $L$  above the flux limit at a given  $z$  are detected. In order to derive the observed data likelihood function, it is necessary to take the survey’s selection method into account. This is done by first deriving the joint likelihood function of both the observed and unobserved data, and then integrating out the unobserved data.

Because the data points are independent, the likelihood function for all  $N$  sources in the universe is

$$p(L, z|\theta) = \prod_{i=1}^N p(L_i, z_i|\theta). \quad (2)$$

<sup>1</sup> We use the terms probability density and probability distribution interchangeably.

In reality, we do not know the luminosities and redshifts for all  $N$  sources, nor do we know the value of  $N$ , as our survey only covers a fraction of the sky and is subject to a selection function. As a result, our survey only contains  $n$  sources. Because of this, the selection process must also be included in the probability model, and the total number of sources,  $N$ , is an additional parameter that needs to be estimated.

We can incorporate the sample selection into the likelihood function by including the random detection of sources. We introduce an  $N$ -element indicator vector  $\mathbf{I}$  that takes on the values  $I_i = 1$  if the  $i^{\text{th}}$  source is included in our survey and  $I_i = 0$  otherwise. Note that  $\mathbf{I}$  is a vector of size  $N$  containing only ones and zeros. In this case, the selection function is the probability of including a source given  $L$  and  $z$ ,  $p(I_i = 1|L_i, z_i)$ . The complete data likelihood is then the probability that all objects of interest in the universe (e.g., all quasars) have luminosities  $L_1, \dots, L_N$  and redshifts  $z_1, \dots, z_N$ , and that the selection vector  $I$  has the values  $I_1, \dots, I_N$ , given our assumed luminosity function:

$$p(L, z, \mathbf{I}|\theta, N) = C_n^N \prod_{i \in \mathcal{A}_{obs}} p(I_i = 1|L_i, z_i) p(L_i, z_i|\theta) \prod_{j \in \mathcal{A}_{mis}} p(I_j = 0|L_j, z_j) p(L_j, z_j|\theta). \quad (3)$$

Here,  $C_n^N = N!/n!(N-n)!$  is the binomial coefficient,  $\mathcal{A}_{obs}$  denotes the set of  $n$  included sources, and  $\mathcal{A}_{mis}$  denotes the set of  $N-n$  missing sources. The number of sources detected in a survey is random, and therefore the binomial coefficient is necessary in normalizing the likelihood function, as it gives the number of possible ways to select a subset of  $n$  sources from a set of  $N$  total sources.

Because we are interested in the probability of the observed data, given our assumed model, the complete data likelihood function is of little use by itself. However, we can integrate Equation (3) over the missing data to obtain the observed data likelihood function. This is because the marginal probability distribution of the observed data is obtained by integrating the joint probability distribution of the observed and the missing data over the missing data:

$$p(L_{obs}, z_{obs}, \mathbf{I}|\theta, N) = C_n^N \prod_{i \in \mathcal{A}_{obs}} p(I_i = 1|L_i, z_i) p(L_i, z_i|\theta) \quad (4)$$

$$\times \prod_{j \in \mathcal{A}_{mis}} \int_0^\infty \int_0^\infty p(I_j = 0|L_j, z_j) p(L_j, z_j|\theta) dL_j dz_j \quad (5)$$

$$\propto C_n^N [p(I = 0|\theta)]^{N-n} \prod_{i \in \mathcal{A}_{obs}} p(L_i, z_i|\theta), \quad (6)$$

where the probability that the survey misses a source, given the parameters  $\theta$ , is

$$p(I = 0|\theta) = \int \int p(I = 0|L, z) p(L, z|\theta) dL dz. \quad (7)$$

Here, we have introduced the notation that  $L_{obs}$  and  $z_{obs}$  denote the set of values of  $L$  and  $z$  for those sources included in one's survey, and we have omitted terms that do not depend on  $\theta$  or  $N$  from Equation (6). Equation (6) is the observed data likelihood function, given an assumed luminosity function (Eq.[1]). Qualitatively, the observed data likelihood function is the probability of observing the set of  $n$  luminosities  $L_1, \dots, L_n$  and redshifts  $z_1, \dots, z_n$  given the assumed luminosity function parameterized by  $\theta$ , multiplied by the probability of not detecting  $N-n$  sources given  $\theta$ , multiplied by the number of ways of selecting a subset of  $n$  sources from a set of  $N$  total sources. The observed data likelihood function can be used to calculate a maximum likelihood estimate of the luminosity function, or combined with a prior distribution to perform Bayesian inference.

### 2.3. Comparison with the Poisson Likelihood

The observed data likelihood given by Equation (6) differs from that commonly used in the luminosity function literature. Instead, a likelihood based on the Poisson distribution is often used. Marshall et al. (1983) give the following equation for the log-likelihood function based on the Poisson distribution:

$$\log p(L_{obs}, z_{obs}|\theta, N) = \sum_{i \in \mathcal{A}_{obs}} \log \phi(L_i, z_i|N, \theta) + \int \int p(I = 1|L, z) \phi(L, z|\theta, N) \frac{dV}{dz} dL dz. \quad (8)$$

Inserting Equation (1) for  $\phi(L, z|\theta)$ , the log-likelihood based on the Poisson likelihood becomes

$$\log p(L_{obs}, z_{obs}|\theta, N) = n \log N + \sum_{i \in \mathcal{A}_{obs}} \log p(L_i, z_i|\theta) - N p(I = 1|\theta), \quad (9)$$

where,  $p(I = 1|\theta) = 1 - p(I = 0|\theta)$ , and  $p(I = 0|\theta)$  is given by Equation (7). In contrast, the log-likelihood we have derived based on the binomial distribution is the logarithm of Equation (6):

$$\log p(L_{obs}, z_{obs}|\theta, N) = \log N! - \log n! - \log(N-n)! + \sum_{i \in \mathcal{A}_{obs}} \log p(L_i, z_i|\theta) + (N-n) \log p(I = 0|\theta). \quad (10)$$

The likelihood functions implied by Equations (9) and (10) are functions of  $N$ , and thus the likelihoods may also be maximized with respect to the LF normalization. This is contrary to what is often claimed in the literature, where

the LF normalization is typically chosen to make the expected number of sources observed in one's survey equal to the actual number observed.

The binomial likelihood, given by Equation (6), contains the term  $C_n^N$ , resulting from the fact that the total number of sources included in a survey,  $n$ , follows a binomial distribution. For example, suppose one performed a survey over one quarter of the sky with no flux limit. Assuming that sources are uniformly distributed on the sky, the probability of including a source for this survey is simply  $1/4$ . If there are  $N$  total sources in the universe, the total number of sources that one would find within the survey area follows a binomial distribution with  $N$  'trials' and probability of 'success'  $p = 1/4$ . However, the Poisson likelihood is derived by noting that the number of sources detected in some small bin in  $(L, z)$  follows a Poisson distribution. Since the sum of a set of Poisson distributed random variables also follows a Poisson distribution, this implies that the total number of sources detected in one's survey,  $n$ , follows a Poisson distribution. However,  $n$  actually follows a binomial distribution, and thus the observed data likelihood function is not given by the Poisson distribution. The source of this error is largely the result of approximating the number of sources in a bin as following a Poisson distribution, when in reality it follows a binomial distribution.

Although the Poisson likelihood function for the LF is incorrect, the previous discussion should not be taken as a claim that previous work based on the Poisson likelihood function is incorrect. When the number of sources included in one's sample is much smaller than the total number of sources in the universe, the binomial distribution is well approximated by the Poisson distribution. Therefore, if the survey only covers a small fraction of the sky, or if the flux limit is shallow enough such that  $n \ll N$ , then the Poisson likelihood function should provide an accurate approximation to the true binomial likelihood function. When this is true, statistical inference based on the Poisson likelihood should only exhibit negligible error, so long as there are enough sources in one's survey to obtain an accurate estimate of the LF normalization. In § 3.3 we use simulate to compare results obtained from the two likelihood functions, and to compare the maximum-likelihood approach to the Bayesian approach.

### 3. POSTERIOR DISTRIBUTION FOR THE LF PARAMETERS

We can combine the likelihood function for the LF with a prior probability distribution on the LF parameters to perform Bayesian inference on the LF. The result is the posterior probability distribution of the LF parameters, i.e., the probability distribution of the LF parameters given our observed data. This is in contrast to the maximum likelihood approach, where the maximum likelihood approach seeks to relate the observed value of the MLE to the true parameter value through an estimate of the sampling distribution of the MLE. In Appendix § A we give a more thorough introduction to the difference between the maximum likelihood and Bayesian approaches.

#### 3.1. Derivation of the Posterior Probability Distribution

The posterior probability distribution of the model parameters is related to the likelihood function and the prior probability distribution as

$$p(\theta, N | L_{obs}, z_{obs}, \mathbf{I}) \propto p(\theta, N) p(L_{obs}, z_{obs}, \mathbf{I} | \theta, N), \quad (11)$$

where  $p(\theta, N)$  is the prior on  $(\theta, N)$ , and  $p(L_{obs}, z_{obs}, \mathbf{I} | \theta, N)$  is the observed data likelihood function, given by Equation (6). The posterior distribution is the probability distribution of  $\theta$  and  $N$ , given the observed data,  $L_{obs}$  and  $z_{obs}$ . Because the luminosity function depends on the parameters  $\theta$  and  $N$ , the posterior distribution of  $\theta$  and  $N$  can be used to obtain the probability distribution of  $\phi(L, z)$ , given our observed set of luminosities and redshifts.

It is of use to decompose the posterior as  $p(\theta, N | L_{obs}, z_{obs}) \propto p(N | L_{obs}, z_{obs}) p(\theta | L_{obs}, z_{obs})$ ; here we have dropped the explicit conditioning on  $\mathbf{I}$ . This decomposition separates the posterior into the conditional posterior of the LF normalization at a given  $\theta$ ,  $p(N | L_{obs}, z_{obs}, \theta)$ , from the marginal posterior of the LF shape,  $p(\theta | L_{obs}, z_{obs})$ . In this work we assume that  $N$  and  $\theta$  are independent in their prior distribution,  $p(\theta, N) = p(N) p(\theta)$ , and that the prior on  $N$  is uniform over  $\log N$ . A uniform prior on  $\log N$  corresponds to a prior distribution on  $N$  of  $p(N) \propto 1/N$ , as  $p(\log N) d \log N = p(N) dN$ . Under this prior, one can show that the marginal posterior probability distribution of  $\theta$  is

$$p(\theta | L_{obs}, z_{obs}) \propto p(\theta) [p(I = 1 | \theta)]^{-n} \prod_{i \in \mathcal{A}_{obs}} p(L_i, z_i | \theta), \quad (12)$$

where  $p(I = 1 | \theta) = 1 - p(I = 0 | \theta)$ . We derive Equation (12) in Appendix § B (see also Gelman et al. 2004). Under the assumption of a uniform prior on  $\theta$ , Equation (12) is equivalent to Equation (22) in Fan et al. (2001), who use a different derivation to arrive at a similar result.

Under the prior  $p(\log N) \propto 1$ , the conditional posterior distribution of  $N$  at a given  $\theta$  is a negative binomial distribution with parameters  $n$  and  $p(I = 1 | \theta)$ . The negative binomial distribution gives the probability that the total number of sources in the universe is equal to  $N$ , given that we have observed  $n$  sources in our sample with probability of inclusion  $p(I = 1 | \theta)$ :

$$p(N | n, \theta) = C_{n-1}^{N-1} [p(I = 1 | \theta)]^n [p(I = 0 | \theta)]^{N-n}. \quad (13)$$

Here,  $p(I = 0 | \theta)$  is given by Equation (7) and  $p(I = 1 | \theta) = 1 - p(I = 0 | \theta)$ . Further description of the negative binomial distribution is given in § C. The complete joint posterior distribution of  $\theta$  and  $N$  is then the product of Equations (12) and (13),  $p(\theta, N | L_{obs}, z_{obs}) \propto p(N | \theta, n) p(\theta | L_{obs}, z_{obs})$ .

Because it is common to fit a luminosity function with a large number of parameters, it is computationally intractable to directly calculate the posterior distribution from Equations (12) and (13). In particular, the number of grid points

needed to calculate the posterior will scale exponentially with the number of parameters. Similarly, the number of integrals needed to calculate the marginal posterior probability distribution of a single parameters will also increase exponentially with the number of parameters. Instead, Bayesian inference is most easily performed by simulating random draws of  $N$  and  $\theta$  from their posterior probability distribution. Based on the decomposition  $p(\theta, N|L_{obs}, z_{obs}) \propto p(N|n, \theta)p(\theta|L_{obs}, z_{obs})$ , we can obtain random draws of  $(\theta, N)$  from the posterior by first drawing values of  $\theta$  from Equation (12). Then, for each draw of  $\theta$ , we draw a value of  $N$  from the negative binomial distribution. The values of  $N$  and  $\theta$  can then be used to compute the values of luminosity function via Equation (1). The values of the LF computed from the random draws of  $N$  and  $\theta$  are then treated as a random draw from the probability distribution of the LF, given the observed data. These random draws can be used to estimate posterior means and variances, confidence intervals, and histogram estimates of the marginal distributions. Random draws for  $\theta$  may be obtained via Markov chain Monte Carlo (MCMC) methods, described in § 5, and we describe in § C how to obtain random draws from the negative binomial distribution. In § 6.2 we give more details on using random draws from the posterior to perform statistical inference on the LF.

### 3.2. Illustration of the Bayesian Approach: Schechter Function

Before moving to more advanced models, we illustrate the Bayesian approach by applying it to a simulated set of luminosities drawn from a Schechter function. We do this to give an example of how to calculate the posterior distribution, how to obtain random draws from the posterior and use these random draws to draw scientific conclusions based on the data, and to compare the Bayesian approach with the maximum-likelihood approach (see § 3.3). The Schechter luminosity function is:

$$\phi(L) = \frac{N}{L^* \Gamma(\alpha + 1)} \left( \frac{L}{L^*} \right)^\alpha e^{-L/L^*}, \quad \theta = (\alpha, L^*). \quad (14)$$

For simplicity, we ignore a  $z$  dependence. The Schechter function is equivalent to a Gamma distribution with shape parameter  $k = \alpha + 1$ , and scale parameter  $L^*$ . Note that  $k > 0$  and  $\alpha > -1$ ; otherwise the integral of Equation (14) may be negative or become infinite. For our simulation, we randomly draw  $N = 1000$  galaxy luminosities from Equation (14) using a value of  $\alpha = 0$  and  $L^* = 10^{44}$  erg s $^{-1}$ .

To illustrate how the results depend on the detection limit, we placed two different detection limits on our simulated survey. The first limit was at  $L_{min} = 2 \times 10^{43}$  ergs s $^{-1}$ , and the second was at  $L_{min} = 2 \times 10^{44}$  ergs s $^{-1}$ . We used a hard detection limit, where all sources above  $L_{min}$  were detected and all sources below  $L_{min}$  were not:  $p(I = 1|L > L_{min}) = 1$  and  $p(I = 1|L < L_{min}) = 0$ . Note that the first detection limit lies below  $L^*$ , while the second detection limit lies above  $L^*$ . We were able to detect  $n \sim 818$  sources for  $L_{min} = 2 \times 10^{43}$  ergs s $^{-1}$  and  $n \sim 135$  sources for  $L_{min} = 2 \times 10^{44}$  ergs s $^{-1}$ .

The marginal posterior distribution of  $\alpha$  and  $L^*$  can be calculated by inserting into Equation (12) an assumed prior probability distribution,  $p(\alpha, L^*)$ , and the likelihood function,  $p(L_i|\alpha, L^*)$ . Because we are ignoring redshift in our example, the likelihood function is simply  $p(L_i|\alpha, L^*) = \phi(L)/N$ . In this example, we assume a uniform prior on  $\log L^*$  and  $\alpha$ , and therefore  $p(L^*, \alpha) \propto 1/L^*$ . From Equations (12) and (14), the marginal posterior distribution of the parameters is

$$p(\alpha, L^*|L_{obs}) \propto \frac{1}{L^*} [p(I = 1|\alpha, L^*)]^{-n} \prod_{i=1}^n \frac{1}{L^* \Gamma(\alpha + 1)} \left( \frac{L_i}{L^*} \right)^\alpha e^{-L_i/L^*}, \quad (15)$$

where the survey detection probability is

$$p(I = 1|\alpha, L^*) = \int_{L_{min}}^{\infty} \frac{1}{L^* \Gamma(\alpha + 1)} \left( \frac{L_i}{L^*} \right)^\alpha e^{-L_i/L^*} dL. \quad (16)$$

The conditional posterior distribution of  $N$  at a given  $\theta$  is given by inserting in Equation (16) into Equation (13), and the joint posterior of  $\alpha, L^*$ , and  $N$  is obtained by multiplying Equation (15) by Equation (13).

We perform statistical inference on the LF by obtaining random draws from the posterior distribution. In order to calculate the marginal posterior distributions,  $p(\alpha|L_{obs})$ ,  $p(L^*|L_{obs})$ , and  $p(N|L_{obs})$ , we would need to numerically integrate the posterior distribution over the other two parameters. For example, in order to calculate the marginal posterior of  $\alpha$ ,  $p(\alpha|L_{obs}, z_{obs})$ , we would need to integrate  $p(\alpha, L^*, N|L_{obs})$  over  $L^*$  and  $N$  on a grid of values for  $\alpha$ . While feasible for the simple 3-dimensional problem illustrated here, it is faster to simply obtain a random draw of  $\alpha, L^*$ , and  $N$  from the posterior, and then use a histogram to estimate  $p(\alpha|L_{obs})$ . Further details are given in § 6.2 on performing Bayesian inference using random draws from the posterior.

We used the Metropolis-Hastings algorithm described in § 5.1 to obtain a random draw of  $\alpha, L^*$ , and  $N$  from the posterior probability distribution. The result was a set of  $10^5$  random draws from the posterior probability distribution of  $\alpha, L^*$ , and  $N$ . In Figure 1 we show the estimated posterior distribution of  $\alpha, L^*$ , and  $N$  for both detection limits. While  $L^*$  is fairly well constrained for both detection limits, the uncertainties on  $\alpha$  and  $N$  are highly sensitive to whether the detection limit lies above or below  $L^*$ . In addition, the uncertainties on these parameters are not Gaussian, as is often assumed for the MLE.

The random draws of  $\alpha, L^*$ , and  $N$  can also be used to place constraints on the LF. This is done by computing Equation (14) for each of the random draws of  $\alpha, L^*$ , and  $N$ , and plotting the regions that contain, say, 90% of the

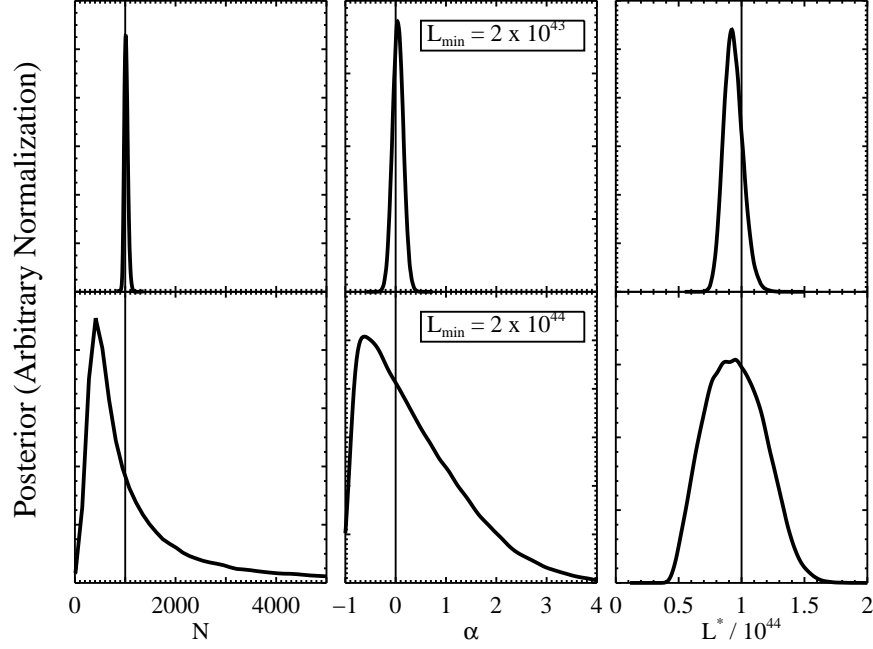


FIG. 1.— Posterior probability distribution of the Schechter luminosity function parameters,  $N$ ,  $\alpha$ , and  $L^*$ , for the simulated sample described in § 3.2. The top three panels show the posterior when the luminosity limit of the survey is  $L > 2 \times 10^{43}$  [erg s $^{-1}$ ], and the bottom three panels show the posterior distribution when the luminosity limit of the survey is  $L > 2 \times 10^{44}$  [erg s $^{-1}$ ]. The vertical lines mark the true values of the parameters,  $N = 1000$ ,  $\alpha = 0$ , and  $L^* = 10^{44}$  [erg s $^{-1}$ ]. The uncertainty on the parameters increases considerably when  $L_{min} > L^*$ , reflecting the fact that the bright end of the Schechter LF contains little information on  $\alpha$  or  $N$ .

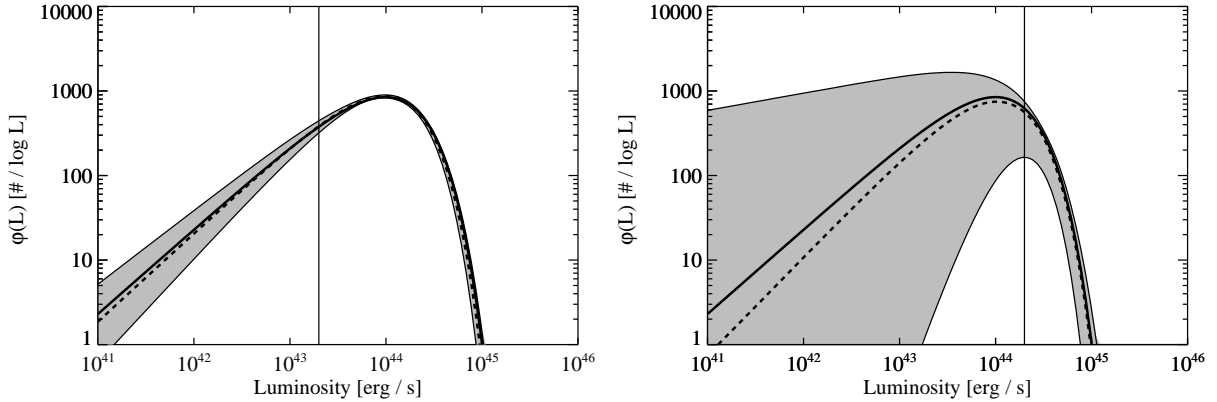


FIG. 2.— True value of the Schechter luminosity function (dashed line), compared with the best fit luminosity function calculated from the posterior median of the Schechter function parameters,  $N$ ,  $\alpha$ , and  $L^*$  (solid line), from the simulated sample described in § 3.2. The left panel summarizes the posterior probability distribution of the LF when the luminosity limit is  $L > 2 \times 10^{43}$  [erg s $^{-1}$ ], and the right panel summarizes the posterior distribution of the LF when the luminosity limit is  $L > 2 \times 10^{44}$  [erg s $^{-1}$ ]. In both panels the shaded region contains 90% of the posterior probability, and the vertical line marks the lower luminosity limit of the simulated survey. The uncertainty on the LF below the luminosity limit increases considerably when  $L_{min} > L^*$ , reflecting the fact that the bright end of the Schechter LF contains little information on  $\alpha$  or  $N$ , and therefore contains little information on the faint end of the LF.

probability. In Figure 2 we show the posterior median estimate of the LF, as well as the region containing 90% of the posterior probability. As can be seen, the 90% bounds contain the true value of the LF, and increase or decrease to reflect the amount of data available as a function of  $L$ . Furthermore, unlike the traditional MLE, these bounds do not rely on an assumption of Gaussian uncertainties, and therefore the confidence regions are valid for any sample size.

### 3.3. Comparison with Maximum-likelihood: Schechter Function

We also use Monte Carlo simulation to compare the Bayesian approach to maximum-likelihood for both the binomial and Poisson likelihood functions. We simulated 20 data sets for four types of surveys: (1) A large area shallow survey,

TABLE 1  
SCHECHTER FUNCTION CONFIDENCE INTERVALS: MAXIMUM-LIKELIHOOD VS. BAYESIAN  
INFERENCE

	Large Area, Shallow	Large Area, Medium	Small Area, Deep	Rare Object
Normalization, $N$				
Poisson	19	16	10	11
Binomial	19	19	12	10
Bayesian	20	19	19	20
Faint End Power-law Slope, $k$				
Poisson	18	17	18	17
Binomial	18	19	18	18
Bayesian	20	20	18	19
Bright End Exponential Cut-off, $L^*$				
Poisson	20	19	19	18
Binomial	20	20	19	18
Bayesian	20	20	18	20

NOTE. — Table 1 gives the number of times the true value of each parameter was contained within the estimated 95% confidence interval for the simulated data sets described in § 3.3. The results are reported separately for each type of survey and Schechter function parameter. We simulated 20 data sets for each type of survey.

(2) a large area medium depth survey, (3) a small area deep survey, and (4) a large area deep survey for rare objects, such as  $z \sim 6$  quasars (e.g., Fan et al. 2006). For all four survey types we simulated quasars from a Schechter luminosity function with parameters the same as in § 3.2. For the large area shallow survey we used a total number of sources of  $N = 10^5$ , an area of  $\Omega = 10^4 \text{ deg}^2$ , and a lower luminosity limit of  $L_{\min} = 5 \times 10^{44} \text{ erg s}^{-1}$ . Only  $n \sim 160$  sources are expected to be detected by this survey. For the large area medium depth survey we also used a LF normalization of  $N = 10^5$  and area of  $\Omega = 10^4 \text{ deg}^2$ , but instead used a lower luminosity limit of  $L_{\min} = 5 \times 10^{43} \text{ erg s}^{-1}$ . The large area medium depth survey is expected to detect  $n \sim 1.5 \times 10^4$  sources. For the small area deep survey we used a survey area of  $\Omega = 448 \text{ arcmin}^2$ , a LF normalization of  $N = 5 \times 10^7$  sources, and a lower luminosity limit of  $L_{\min} = 10^{43} \text{ erg s}^{-1}$ . This survey is expected to detect  $n \sim 140$  sources. Finally, for the large area deep rare object survey we used an area of  $\Omega = 10^4 \text{ deg}^2$ , a LF normalization of  $N = 75$  sources, and a lower luminosity limit of  $L_{\min} = 10^{43} \text{ erg s}^{-1}$ . Only  $n \sim 16$  sources are expected to be detected by the rare object survey.

We fit each of the 20 simulated data sets by maximum-likelihood for both the binomial and Poisson likelihood functions. The 95% confidence intervals on the best-fit parameters were determined using 2000 bootstrap samples. We generate each bootstrap sample by randomly drawing  $n$  data points with replacement from the original sample, and then calculate the maximum-likelihood estimates for each bootstrap sample. We use the bootstrap to estimate the confidence intervals because the bootstrap does not assume that the errors are Gaussian, and because it is a common technique used in the LF literature. We estimate the 95% confidence intervals directly from the 0.025 and 0.975 percentiles of the bootstrap sample. While bootstrap confidence intervals derived in this manner are known to be biased (e.g., Efron 1987; Davison & Hinkley 1997), additional corrections to the bootstrap samples are complicated. In addition, it is common practice to estimate bootstrap confidence intervals in this manner, and it is worth testing their accuracy. For the Bayesian approach, we used the MHA algorithm described in § 5.1 to simulate  $5 \times 10^4$  random draws from the posterior distribution. The MHA algorithm was faster than fitting the 2000 bootstrap samples using maximum likelihood.

For each of the simulated samples, we counted the number of times that the true values of  $N$ ,  $\alpha$ , and  $L^*$  were contained within the estimated 95% confidence interval. The results are summarized in Table 1. Because we estimated values of three parameters for 20 simulated data sets of 4 different types of surveys, we had 240 ‘trials’ with probability of ‘success’  $p = 0.95$ . If the estimated 95% confidence regions corresponded to the true regions, then with  $\approx 99\%$  probability between 220 and 236 of the ‘trials’ would fall within the estimated confidence region. For the binomial likelihood, the true value of a parameter was within the estimated 95% confidence region only 210 times (88%), and for the Poisson likelihood the true value of a parameter was within the estimated 95% confidence region only 202 times (84%). In contrast, the Bayesian approach was able to correctly constrain the true value of a parameter to be within the 95% confidence region 233 times (97%). Therefore, for our simulations confidence regions derived from bootstrapping the maximum-likelihood estimate are too narrow, while the confidence regions derived from the Bayesian method are correct.

Most of the failure in the maximum-likelihood confidence intervals came from the difficulty of the maximum-likelihood approach in constraining the LF normalization,  $N$ , for the small area deep survey and for the rare object survey. In particular, for these two surveys the bootstrap 95% confidence intervals for both the binomial and Poisson likelihood function only contained the true value of  $N$  roughly 50% of the time. In general, there wasn’t a significant difference among the simulated surveys in the ability of the three different statistical approaches to constrain  $k$  and  $L^*$  at 95% confidence. However, the Poisson and binomial likelihood functions gave slightly different results for the larger area



medium depth survey. For this survey the 95% confidence intervals for the maximum-likelihood estimate derived from the Poisson distribution were somewhat smaller than those for the binomial distribution, only correcting including the true values of  $N$ ,  $k$ , and  $L^*$  roughly 85% of the time. This is expected, because the Poisson distribution is the limit of the binomial distribution as the probability of including a source approaches zero; however, the detection probability for the large area medium depth survey is  $\approx 0.15$ .

The results of our simulations imply that the Poisson likelihood function may lead to biased estimates of confidence intervals on the luminosity function parameters, so long as an astronomical survey is able to detect a significant fraction of the objects of interest. Use of the Poisson likelihood function may thus be problematic for the large astronomical surveys becoming common, so long as they are deep enough to achieve a moderate detection fraction. For the simulations performed here, using the Poisson likelihood function resulted in confidence intervals that are too narrow. However, these simulations were for a Schechter luminosity function, and other parameterizations may be affected differently. Considering that there are no obvious computational advantages to using the Poisson likelihood function, we recommend that the correct binomial likelihood function be used, as it is the correct form.

#### 4. MIXTURE OF GAUSSIAN FUNCTIONS MODEL FOR THE LUMINOSITY FUNCTION

In this section we describe a mixture of Gaussian functions model for the luminosity function. The mixture of Gaussians model is a common and well studied ‘non-parametric’ model that allows flexibility when estimating a distribution, and is often employed when there is uncertainty regarding the specific functional form of the distribution of interest. The basic idea is that one can use a suitably large enough number of Gaussian functions to accurately approximate the true LF, even though the individual Gaussians have no physical meaning. In this sense, the Gaussian functions serve as a basis set of the luminosity function. As a result, we avoid the assumption of a more restrictive parametric form, such as a power-law, which can introduce considerable bias when extrapolating beyond the bounds of the observable data. We have not experimented with other luminosity function basis sets, although mixture models are very flexible and need not be limited to Gaussian functions.

In this work we assume the mixture of Gaussian functions for the joint distribution of  $\log L$  and  $\log z$ , as the logarithm of a strictly positive variable tends to more closely follow a normal distribution than does the untransformed variable. Therefore, we expect that a fewer number of Gaussians will be needed to accurately approximate the true LF, thus reducing the number of free parameters. Assuming a mixture of Gaussian functions for the joint distribution of  $\log L$  and  $\log z$  is equivalent to assuming a mixture of log-normal distributions for the distribution of  $L$  and  $z$ . The mixture of  $K$  Gaussian functions model for the  $i^{\text{th}}$  data point is

$$p(\log L_i, \log z_i | \pi, \mu, \Sigma) = \sum_{k=1}^K \frac{\pi_k}{2\pi|\Sigma_k|^{1/2}} \exp \left[ -\frac{1}{2}(\mathbf{x}_i - \mu_k)^T \Sigma_k^{-1} (\mathbf{x}_i - \mu_k) \right], \quad \theta = (\pi, \mu, \Sigma), \quad (17)$$

where  $\sum_{k=1}^K \pi_k = 1$ . Here,  $\mathbf{x}_i = (\log L_i, \log z_i)$ ,  $\mu_k$  is the 2-element mean (i.e., position) vector for the  $k^{\text{th}}$  Gaussian,  $\Sigma_k$  is the  $2 \times 2$  covariance matrix for the  $k^{\text{th}}$  Gaussian, and  $\mathbf{x}^T$  denotes the transpose of  $\mathbf{x}$ . In addition, we denote  $\pi = (\pi_1, \dots, \pi_K)$ ,  $\mu = (\mu_1, \dots, \mu_K)$ , and  $\Sigma = (\Sigma_1, \dots, \Sigma_K)$ . The variance in  $\log L$  for Gaussian  $k$  is  $\sigma_{L,k}^2 = \Sigma_{11,k}$ , the variance in  $\log z$  for Gaussian  $k$  is  $\sigma_{z,k}^2 = \Sigma_{22,k}$ , and the covariance between  $\log L$  and  $\log z$  for Gaussian  $k$  is  $\sigma_{Lz,k} = \Sigma_{12,k}$ . In this work we consider the number of Gaussian components,  $K$ , to be specified by the researcher and fixed. If the number of Gaussian functions is also considered to be a free parameter, then methods exist for performing Bayesian inference on  $K$  as well (e.g., Richardson & Green 1997). Statistical inference on the luminosity functions studied in this work were not sensitive to the choice of  $K$  so long as  $K \geq 3$ , and we conclude that values of  $K \geq 3$  should be sufficient for most smooth and unimodal luminosity functions.

Under the mixture model, the LF can be calculated from Equations (1) and (17). Noting that  $p(L, z) = p(\log L, \log z) / (Lz(\ln 10)^2)$ , the mixture of Gaussian functions model for the LF is

$$\phi(L, z | \theta, N) = \frac{N}{Lz(\ln 10)^2} \left( \frac{dV}{dz} \right)^{-1} \sum_{k=1}^K \frac{\pi_k}{2\pi|\Sigma_k|^{1/2}} \exp \left[ -\frac{1}{2}(\mathbf{x} - \mu_k)^T \Sigma_k^{-1} (\mathbf{x} - \mu_k) \right], \quad (18)$$

where, as before,  $\mathbf{x} = (\log L, \log z)$ . A mixture of Gaussian functions models was also used by Blanton et al. (2003) to estimate the  $z = 0.1$  galaxy LF from the Sloan Digital Sky Survey (SDSS). Our mixture of Gaussian functions model differs from that used by Blanton et al. (2003) in that we do not fix the Gaussian function centroids to lie on a grid of values, and their individual widths are allowed to vary. This flexibility enables us to use a smaller number of Gaussian functions (typically  $\sim 3 - 6$ ) to accurately fit the LF.

##### 4.1. Prior Distribution

In this section we describe the prior distribution that we adopt on the mixture of Gaussian functions parameters. While one may be tempted to assumed a uniform prior on  $\pi, \mu$ , and  $\Sigma$ , this will lead to an improper posterior, i.e., the posterior probability density does not integrate to one (Roeder & Wasserman 1997). Therefore, a uniform prior cannot be used, and we need to develop a more informative prior distribution. Following Roeder & Wasserman (1997), we assume a uniform prior on  $\pi_1, \dots, \pi_K$  under the constraint that  $\sum_{k=1}^K \pi_k = 1$ ; formally, this is a Dirichlet(1, ..., 1)

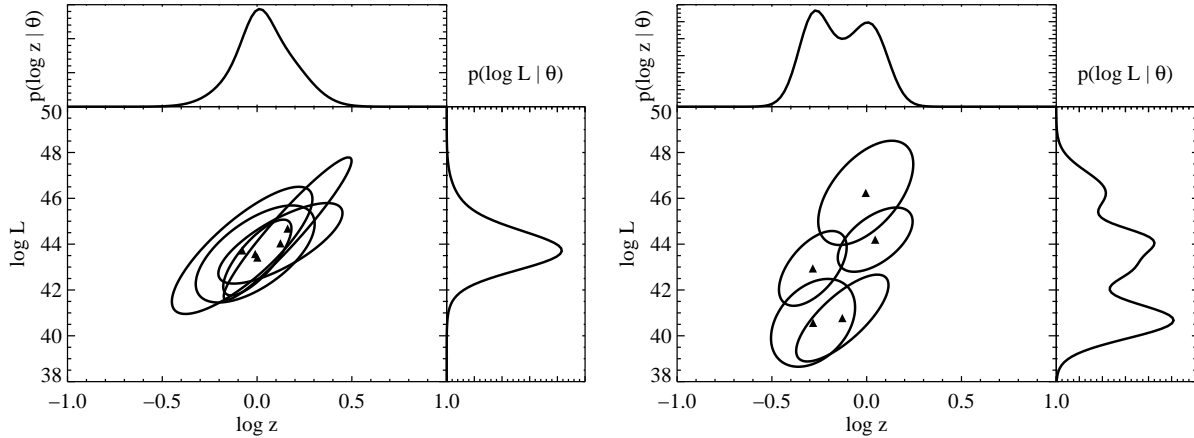


FIG. 3.— An illustration of our prior distribution for the Gaussian function parameters, for  $K = 5$  Gaussian functions. Shown are a case when the Gaussian functions used in modelling the luminosity function are close together with respect to their covariances (left), and when the Gaussian functions are far apart with respect to their covariance matrices (right). The marginal distributions of  $\log L$  are shown above the plots, and the marginal distributions of  $\log z$  are shown to the right of the plots. When the Gaussian functions are close, the LF is unimodal, but when the Gaussian functions are far apart, the LF is multimodal. Because our prior distribution is constructed to place more probability on situations when the Gaussian functions are closer together with respect to their individual covariance matrices, it would place more probability on the situation shown in the left plot *a priori*. Our prior therefore reflects our expectation that the LF should not exhibit multiple peaks (modes).

prior, where  $\text{Dirichlet}(\alpha_1, \dots, \alpha_K)$  denotes a Dirichlet density with parameters  $\alpha_1, \dots, \alpha_K$ . We give further details on the Dirichlet probability distribution in Appendix § C.

Although our prior knowledge of the LF is limited, it is reasonable to assume *a priori* that the LF should be unimodal, i.e., that the LF should not exhibit multiple peaks. Currently, the observed distributions of galaxies and AGN are consistent with this assumption. For galaxies, unimodal luminosity function is implied by simple models of galaxy formation (e.g., Press & Schechter 1974; Schechter 1976), and the luminosity functions for galaxies classified by morphology are not sufficiently separated to create multimodality (e.g., Nakamura et al. 2003; Scarlata et al. 2007). However, the luminosity function for AGN may be bimodal due to the possible existence of two different accretion modes. This is largely due to the fact that the distribution of accretion rates relative to the Eddington rate,  $\dot{m}$ , is likely bimodal (Ho 2002; Marchesini et al. 2004; Hopkins et al. 2006b; Cao & Xu 2007) as a result of a transition from a radiatively inefficient flow to an efficient one at  $\dot{m} \sim 0.01$  (e.g., Jester 2005). Because  $L \propto M_{BH}\dot{m}$ , the distribution of luminosities for AGN may be bimodal. If a survey is unable to detect those AGN in the faint radiatively inefficient mode, then the assumption of unimodality is violated and the estimated AGN luminosity function only refers to those AGN in the bright radiatively efficient mode.

To quantify our prior assumption that the LF is more likely to be unimodal, we construct our prior distribution to place more probability on situations where the individual Gaussian functions are close together in terms of their widths. In addition, we only specify the parametric form of the prior distribution, but allow the parameters of the prior distribution to vary and to be determined by the data. This allows our prior distribution to be flexible enough to have a minimal effect on the final results beyond conveying our prior consideration that the LF should be unimodal. We introduce our prior to place more probability on unimodal luminosity functions, to ensure that the posterior integrates to one, and to aid in convergence of the MCMC. Figure 3 illustrates the general idea that we are attempting to incorporate into our prior distribution. In this figure, we show a situation where the Gaussian functions are close together with respect to their widths, and far apart with respect to their widths. When the distances between the individual Gaussian functions, normalized by their covariance matrices (the measure of their ‘width’), is small, the LF is unimodal; however, when the distances between the Gaussian functions are large with respect to their covariance matrices, the LF exhibits multiple modes. We construct a prior distribution that places less probability on the latter situation.

Our prior on the Gaussian mean vectors and covariance matrices is similar to the prior described by Roeder & Wasserman (1997), but generalized to 2-dimensions. For our prior, we assume an independent multivariate Cauchy distribution for each of the Gaussian means,  $\mu$ , with 2-dimensional mean vector  $\mu_0$  and  $2 \times 2$  scale matrix  $T$ . A Cauchy distribution is equivalent to a student’s  $t$  distributions with 1 degree of freedom, and when used as a function in astronomy and physics it is commonly referred to as a Lorentzian; we describe the Cauchy distribution further in § C of the appendix. The scale matrix is chosen to be the harmonic mean of the Gaussian function covariance matrices:

$$T = \left( \frac{1}{K} \sum_{k=1}^K \Sigma_k^{-1} \right)^{-1}. \quad (19)$$

Qualitatively, this prior means that we consider it more likely that the centroids of the individual Gaussian functions

should scatter about some mean vector  $\mu_0$ , where the width of this scatter should be comparable to the typical width of the individual Gaussian functions. The prior mean,  $\mu_0$ , is left unspecified and is an additional free parameter to be estimated from the data. We choose a Cauchy prior because the Cauchy distribution is heavy tailed, and therefore does not heavily penalize the Gaussian functions for being too far apart. As a result, the Cauchy prior is considered to be robust compared to other choices, such as the multivariate normal distribution.

Because we use a random walk computational technique to explore the parameter space and estimate the posterior distribution, we find it advantageous to impose additional constraints on the Gaussian centroids. Both  $\mu$  and  $\mu_0$  are constrained to the region  $\log L_{low} \leq \mu_{l,k} \leq \log L_{high}$  and  $\log z_{low} \leq \mu_{z,k} \leq \log z_{high}$ , where  $\mu_{l,k}$  is the mean in  $\log L$  for the  $k^{\text{th}}$  Gaussian,  $\mu_{z,k}$  is the mean in  $\log z$  for the  $k^{\text{th}}$  Gaussian. These constraints are imposed to keep the Markov chains (see § 5) from ‘wandering’ into unreasonable regions of the parameter space. The flux limit sets a lower limit on the luminosity of detected sources as a function of  $z$ , and therefore there is nothing in the observed data to ‘tell’ the random walk that certain values of  $\mu_l$  are unreasonable. For example, suppose our survey is only able to detect quasars with  $L \gtrsim 10^{10} L_\odot$ . Because of this, there is nothing in our data, as conveyed through the likelihood function, that says values of, say,  $L \sim 10 L_\odot$  are unreasonable, and thus the Markov chains can get stuck wandering around values of  $\mu_l \sim 1$ . However, we know *a priori* that values of  $\mu_l \sim 1$  are unphysical, and therefore it is important to incorporate this prior knowledge into the posterior, as it is not reflected in the likelihood function. The values of these limits should be chosen to be physically reasonable. As an example, for the SDSS DR3 quasar LF with luminosities measured at  $\lambda L_\lambda(2500\text{\AA})$ , it might be reasonable to take  $L_{low} = 10^{40} \text{ erg s}^{-1}$ ,  $L_{high} = 10^{48} \text{ erg s}^{-1}$ ,  $z_{low} = 10^{-4}$ , and  $z_{high} = 7$ .

Generalizing the prior of Roeder & Wasserman (1997), we assume independent inverse Wishart priors on the individual Gaussian covariance matrices with  $\nu = 1$  degrees of freedom, and common scale matrix  $A$ . We give a description of the Wishart and inverse Wishart distributions in § C. This prior states that the individual  $\Sigma_k$  are more likely to be similar rather than different. The common scale matrix,  $A$ , is left unspecified so it can adapt to the data. As with  $\mu$ , we recommend placing upper and lower limits on the allowable values of dispersion in  $\log L$  and  $\log z$  for each Gaussian.

Mathematically, our prior is

$$p(\pi, \mu, \Sigma, \mu_0, A) \propto \prod_{k=1}^K p(\mu_k | \mu_0, \Sigma) p(\Sigma_k | A) \quad (20)$$

$$\propto \prod_{k=1}^K \text{Cauchy}_2(\mu_k | \mu_0, T) \text{Inv-Wishart}_1(\Sigma_k | A), \quad (21)$$

under the constraints given above. Here,  $\text{Cauchy}_2(\mu_k | \mu_0, T)$  denotes a 2-dimensional Cauchy distribution as a function of  $\mu_k$ , with mean vector  $\mu_0$  and scale matrix  $T$ . In addition,  $\text{Inv-Wishart}_1(\Sigma_k | A)$  denotes an inverse Wishart density as a function of  $\Sigma_k$ , with one degree of freedom and scale matrix  $A$ . We have also experimented with using a uniform prior on the parameters, constricted to some range. In general, this did not change our constraints on the LF above the flux limit, but resulted in somewhat wider confidence regions on the LF below the flux limit. This is to be expected, since our adopted Cauchy prior tends to restrict the inferred LF to be unimodal, and therefore limits the number of possible luminosity functions that are considered to be consistent with the data.

#### 4.2. Posterior Distribution for Mixture of Gaussians Model

Now that we have formulated the prior distribution, we can calculate the posterior distribution for the mixture of Gaussians model of  $\phi(L, z)$ . Because we have formulated the mixture model for the LF in terms of  $\log L$  and  $\log z$ , the marginal posterior distribution of  $\theta$  is

$$p(\theta, \mu_0, A | \log L_{obs}, \log z_{obs}) \propto p(\theta, \mu_0, A) [p(I = 1 | \theta)]^{-n} \prod_{i \in \mathcal{A}_{obs}} p(\log L_i, \log z_i | \theta), \quad \theta = (\pi, \mu, \Sigma), \quad (22)$$

where  $p(\theta, \mu_0, A)$  is given by Equation (21),  $p(\log L_i, \log z_i | \theta)$  is given by Equation (17), and

$$p(I = 1 | \theta) = \int_{-\infty}^{\infty} \int_{-\infty}^{\infty} p(I = 1 | \log L, \log z) p(\log L, \log z | \theta) d \log L d \log z \quad (23)$$

is the probability of including a source, given the model parameters  $\theta$ . The conditional posterior distribution of  $N$  given  $\pi, \mu$ , and  $\Sigma$  is given by inserting Equation (23) into (13). The complete joint posterior distribution is then

$$p(\theta, N, \mu_0, A | \log L_{obs}, \log z_{obs}) \propto p(N | \theta, n) p(\theta, \mu_0, A | \log L_{obs}, \log z_{obs}). \quad (24)$$

### 5. USING MARKOV CHAIN MONTE CARLO TO ESTIMATE THE POSTERIOR DISTRIBUTION OF THE LUMINOSITY FUNCTION

For our statistical model,  $\mu_0$  has 2 free parameters,  $A$  has 3 free parameters, and each of the  $K$  Gaussian components has 6 free parameters. Because the values of  $\pi$  are constrained to sum to one, there are only  $6K - 1$  free parameters for the Gaussian mixture model. The number of free parameters in our statistical model is therefore  $6K + 4$ . The large

number of parameters precludes calculation of the posterior on a grid of  $\pi, \mu, \Sigma, \mu_0, A$ , and  $N$ . Furthermore, the multiple integrals needed for marginalizing the posterior, and thus summarizing it, are numerically intractable. Because of this, we employ Markov Chain Monte Carlo (MCMC) to obtain a set of random draws from the posterior distribution. A Markov chain is a random walk, where the probability distribution of the current location only depends on the previous location. To obtain random numbers generated from the posterior distribution, one constructs a Markov chain that performs a random walk through the parameter space, where the Markov chain is constructed to eventually converge to the posterior distribution. Once convergence is reached, the values of the Markov chain are saved at each iteration, and the values of these locations can be treated as a random draw from the posterior distribution. These draws may then be used to estimate the posterior distribution of  $\phi(L, z)$ , and thus an estimate of the LF and its uncertainty can be obtained.

In this work we use the Metropolis-Hastings algorithm (MHA, Metropolis & Ulam 1949; Metropolis et al. 1953; Hastings 1970) to perform the MCMC. We describe the particular MHA we employ for Bayesian inference on the LF; however for a more general and complete description of the MHA, we refer the reader to Chib & Greenberg (1995) or Gelman et al. (2004). We use the MHA to obtain a set of random draws from the marginal posterior distribution of  $\theta$ , given by Equation (22). Then, given these random draws of  $\theta$ , random draws for  $N$  may be obtained directly from the negative binomial distribution (see Eq.[13] and § C of the appendix).

The basic idea behind the MHA is illustrated in Figure 4 for the special case of a symmetric jumping distribution. First, one starts with an initial guess for  $\theta$ . Then, at each iteration a proposed value of  $\theta$  is randomly drawn from some ‘jumping’ distribution. For example, this jumping distribution could be a normal density with some fixed covariance matrix, centered at the current value of  $\theta$ . Then, if the proposed value of  $\theta$  improves the posterior, it is stored as the new value of  $\theta$ . Otherwise, it is stored as the new value with probability equal to the ratio of the values of the posterior distribution at the proposed and current value of  $\theta$ . If the proposed value of  $\theta$  is rejected, then the value of  $\theta$  does not change, and the current value of  $\theta$  is stored as the ‘new’ value of  $\theta$ . The process is repeated until convergence. If the jumping distribution is not symmetric, then a correction needs to be made to the acceptance rule in order to account for asymmetry in the jumping distribution. A jumping distribution is symmetric when the probability of jumping from a current value  $\theta$  to a new value  $\theta^*$  is the same as jumping from  $\theta^*$  to  $\theta$ . For example, the normal distribution is symmetric, while the log-normal distribution is not.

### 5.1. Metropolis-Hastings Algorithm for Schechter Luminosity Function

Before describing our MHA algorithm for the mixture of Gaussian functions model, we describe a simpler MHA algorithm for the Schechter function model given by Equation (14) in § 3.2. We do this to illustrate the MHA using a more familiar luminosity function. An MHA for obtaining random draws of  $\alpha, L^*$ , and  $N$  from Equation (15) is:

1. Start with an initial value of  $\alpha$  and  $L^*$ , denoted as  $\tilde{\alpha}$  and  $\tilde{L}^*$ . A good initial value is the maximum-likelihood estimate.
2. Draw a proposal value of  $\log L^*$  from a normal distribution centered on the current value of  $\log L^*$ ,  $\log \tilde{L}^*$ . The variance in the jumping distribution of  $\log L^*$  should be fixed at the beginning of the MHA. A larger jumping variance will lead to jumps that travel greater distances, but will then lead to lower MHA acceptance rates. The value of the jumping variance should be tuned to give acceptance rates  $\sim 0.4$ . We use a normal jumping distribution to vary  $\log L^*$  because  $\log L^*$  is defined on  $(-\infty, \infty)$ , while  $L^*$  is only defined on  $(0, \infty)$ . While we could use a jumping distribution to directly vary  $L^*$ , it is not always easy to simulate random variables directly from distributions that are only defined for  $L^* > 0$ .

Denoting the proposal value of  $L^*$  as  $\hat{L}^*$ , calculate the ratio

$$r_{L^*} = \frac{\hat{L}^* p(\tilde{\alpha}, \hat{L}^* | L_{obs})}{\tilde{L}^* p(\tilde{\alpha}, \tilde{L}^* | L_{obs})} \quad (25)$$

Here,  $p(\alpha, L^* | L_{obs})$  is the posterior distribution for the Schechter function, given by Equation (15). If  $r_{L^*} > 1$ , then keep the proposal and set  $\tilde{L}^* = \hat{L}^*$ . If  $r_{L^*} < 1$ , then draw a random number  $u$  uniformly distributed between 0 and 1. If  $u < r_{L^*}$ , then keep the proposal and set  $\tilde{L}^* = \hat{L}^*$ . Otherwise, the proposal is rejected and the value of  $\tilde{L}^*$  is unchanged. The factor of  $\hat{L}^*/\tilde{L}^*$  is necessary in Equation (25) in order to correct for the asymmetry in the log-normal jumping distribution.

3. Draw a proposal value of  $\log k = \log(\alpha + 1)$  from a normal distribution centered at the current value of  $\log k$ ,  $\log \tilde{k} = \log(\tilde{\alpha} + 1)$ . Similar to the MHA step for  $L^*$ , we use a normal jumping distribution to vary  $\log k$  because  $\log k$  is defined on  $(-\infty, \infty)$ , while  $\alpha$  is only defined on  $(-1, \infty)$ .

Denoting the proposal value of  $k$  as  $\hat{k}$ , the proposal value of  $\hat{\alpha}$  is  $\hat{\alpha} = \hat{k} - 1$ . Using the values of  $\tilde{\alpha}$  and  $\hat{\alpha}$ , calculate the ratio

$$r_{\alpha} = \frac{\hat{k} p(\hat{\alpha}, \tilde{L}^* | L_{obs})}{\tilde{k} p(\tilde{\alpha}, \tilde{L}^* | L_{obs})} \quad (26)$$

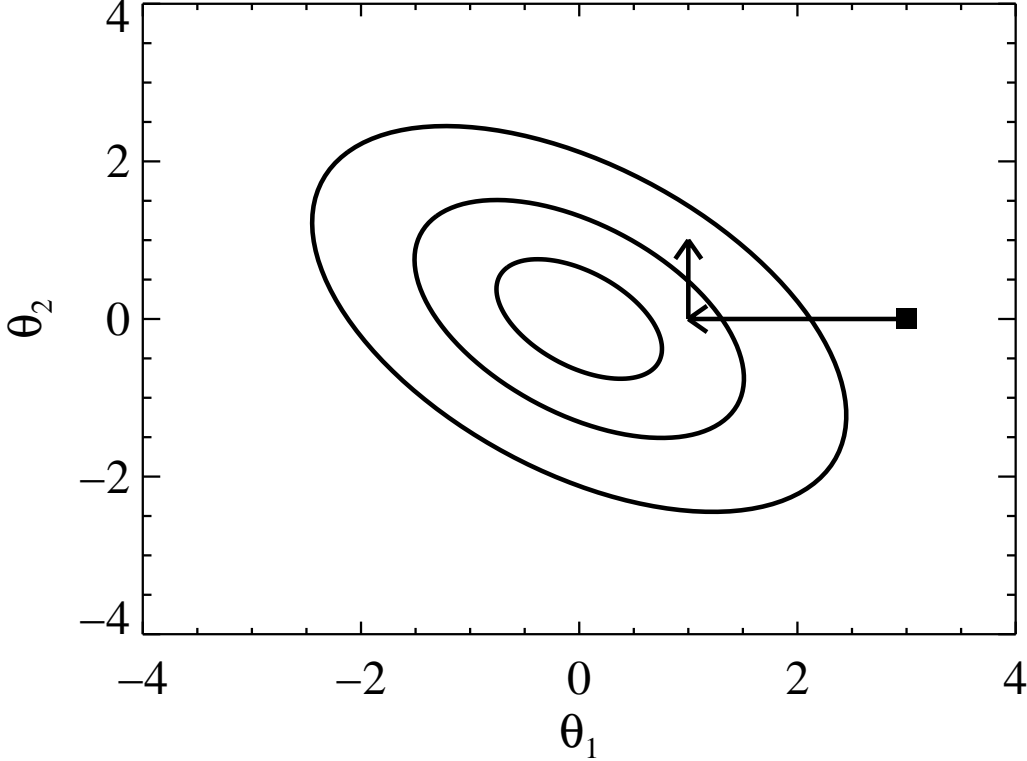


FIG. 4.— Schematic diagram illustrating the random walk Metropolis-Hastings algorithm. The posterior probability distribution is illustrated by the contours, and the random walk is initially at the position marked with a square. A new proposed value of  $\theta_1$  is randomly drawn, marked by the arrow pointing to the left. Because the proposed value of  $\theta_1$  is at a location with higher posterior probability, the new value of  $\theta_1$  is saved, and the random walk ‘jumps’ to the position marked by the arrow. Then, a new proposal for  $\theta_2$  is randomly drawn, marked by the arrow pointing upward. Because this proposed value of  $\theta_2$  is at a location with lower posterior probability, it is only accepted with probability equal to the ratio of the values of the posterior at the proposed position and the current position. If the proposed value is kept, then the new value of  $\theta_2$  is saved, otherwise the current value of  $\theta_2$  is saved. Next, a proposed value of  $\theta_1$  is randomly drawn, and the process repeats, creating a random walk through the parameter space. Because the amount of time that the random walk spends in any given bin in  $\theta_1$  and  $\theta_2$  is proportional to the posterior probability distribution, after the random walk has converged, the values of  $\theta_1$  and  $\theta_2$  from the random walk may be treated as a random draw from the posterior distribution.

If  $r_\alpha > 1$ , then keep the proposal and set  $\tilde{\alpha} = \hat{\alpha}$ . If  $r_\alpha < 1$ , then draw a random number  $u$  uniformly distributed between 0 and 1. If  $u < r_\alpha$ , then keep the proposal and set  $\tilde{\alpha} = \hat{\alpha}$ . Otherwise, the proposal is rejected and the value of  $\tilde{\alpha}$  is unchanged. As with the MHA step for  $L^*$ , the factor of  $\hat{k}/\tilde{k}$  is necessary in Equation (26) in order to correct for the asymmetry in the log-normal jumping distribution.

4. Repeat steps (2)–(3) until the MHA algorithm converges. Techniques for monitoring convergence are described in Gelman et al. (2004). After convergence, use Equation (13) to directly simulate random draws of the LF normalization,  $N$ , for each simulated value of  $\alpha$  and  $L^*$  obtained from the above random walk. Equation (13) has the form of a negative binomial distribution, and a method for simulated random variables from the negative binomial distribution is described in § C of the appendix.

### 5.2. Metropolis-Hastings Algorithm for the Mixture of Gaussian Functions Luminosity Function

Our MHA for the mixture of Gaussian functions model is a more complex version of that used for the Schechter function model. As before, we denote the current value of a parameter by placing a  $\sim$  over its symbol, and we denote the proposed value by placing a  $\hat{\cdot}$  over its symbol. For example, if one were updating  $\pi$ , then  $\tilde{\pi}$  denotes the current value of  $\pi$  in the random walk, and  $\hat{\pi}$  denotes the proposed value of  $\pi$ . We will only update one parameter at a time, so, if we are drawing a proposal for  $\pi$ , the current value of  $\theta$  is denoted as  $\tilde{\theta} = (\tilde{\pi}, \tilde{\mu}, \tilde{\Sigma})$ , and the proposed value of  $\theta$  is denoted as  $\hat{\theta} = (\hat{\pi}, \tilde{\mu}, \tilde{\Sigma})$ .

Our MHA for the mixture of Gaussian functions model is:

1. Start with initial guesses for  $\pi, \mu, \Sigma, \mu_0, A$ , and  $T$ .
2. Draw a proposal value for  $\pi$  from a Dirichlet( $\tilde{g}_1, \dots, \tilde{g}_K$ ) density, where  $\tilde{g}_k = c_\pi n \tilde{\pi}_k + 1$ ,  $n$  is the number of sources in the survey, and  $c_\pi$  is a fixed positive constant that controls how far the ‘jumps’ in  $\pi$  go. Because  $c_\pi$

controls the variance of the Dirichlet density, a smaller value of  $c_\pi$  produces values of  $\hat{\pi}$  that are further from  $\tilde{\pi}$ . The value of  $c_\pi$  should be chosen so that about 15–40% of the MHA proposals are accepted.

After drawing a proposal for  $\pi$ , calculate the value of the posterior distribution at the new value of  $\theta$ ,  $\hat{\theta}$ , and at the old value of  $\theta$ ,  $\tilde{\theta}$ . Then, use these values to calculate the ratio

$$r_\pi = \frac{\text{Dirichlet}(\tilde{\pi}|\hat{g}) p(\hat{\theta}|L_{obs}, z_{obs})}{\text{Dirichlet}(\hat{\pi}|\hat{g}) p(\tilde{\theta}|L_{obs}, z_{obs})}, \quad (27)$$

where  $\hat{g} = c_\pi n \hat{\pi}_1 + 1, \dots, c_\pi n \hat{\pi}_K + 1$ . The ratio of Dirichlet densities in Equation (27) corrects the MHA acceptance rule for the asymmetry in the Dirichlet jumping distribution. If  $r_\pi \geq 1$  then keep the proposed value of  $\pi$ :  $\tilde{\pi} = \hat{\pi}$ . Otherwise keep the proposal with probability  $r_\pi$ . This is done by drawing a uniformly distributed random variable between 0 and 1, denoted by  $u$ . If  $u < r_\pi$ , then set  $\tilde{\pi} = \hat{\pi}$ . If  $u > r_\pi$  then keep the current value of  $\pi$ .

Methods for simulating from the Dirichlet distribution, as well as the functional form of the Dirichlet distribution, are given in § C.

3. For each Gaussian function, draw a proposal for  $\mu_k$  by drawing  $\hat{\mu}_k \sim N_2(\tilde{\mu}_k, V_k)$ , where  $V_k$  is some set covariance matrix. Because the jumping density is symmetric, the MHA acceptance ratio is just given by the ratio of the posterior distributions at the proposed and current value of  $\mu_k$ :  $r_\mu = p(\hat{\theta}|L_{obs}, z_{obs})/p(\tilde{\theta}|L_{obs}, z_{obs})$ . If  $r_\mu \geq 1$  then set  $\tilde{\mu}_k = \hat{\mu}_k$ , otherwise set  $\tilde{\mu}_k = \hat{\mu}_k$  with probability  $r_\mu$ . The MHA update should be performed separately for each Gaussian. The covariance matrix of the jumping kernel,  $V_k$ , should be chosen such that  $\sim 30\%$  of the MHA jumps are accepted.

Since we have constructed the prior distribution with the constraint  $\log L_{low} \leq \mu_{l,k} \leq \log L_{high}$  and  $\log z_{min} \leq \mu_{z,k} \leq \log z_{high}$  for all  $k$ , any values of  $\hat{\mu}_k$  that fall outside of this range should automatically be rejected.

4. For each Gaussian, draw a proposal for  $\Sigma_k$  by drawing  $\hat{\Sigma}_k \sim \text{Wishart}_{\nu_k}(\tilde{\Sigma}_k/\nu_k)$ , where  $\nu_k$  is some set degrees of freedom. Larger values of  $\nu_k$  will produce values of  $\hat{\Sigma}_k$  that are more similar to  $\tilde{\Sigma}_k$ . The MHA acceptance ratio is

$$r_\Sigma = \left( \frac{|\tilde{\Sigma}_k|}{|\hat{\Sigma}_k|} \right)^{\nu_k - 3/2} \exp \left\{ -\frac{\nu_k}{2} \text{tr} \left[ (\hat{\Sigma}_k)^{-1} \tilde{\Sigma}_k - \tilde{\Sigma}_k^{-1} \hat{\Sigma}_k \right] \right\} \frac{p(\hat{\theta}|x_{obs})}{p(\tilde{\theta}|x_{obs})}, \quad (28)$$

where  $\text{tr}(\cdot)$  denotes the trace of a matrix. If  $r_\Sigma \geq 1$  then set  $\tilde{\Sigma}_k = \hat{\Sigma}_k$ , otherwise set  $\tilde{\Sigma}_k = \hat{\Sigma}_k$  with probability  $r_\Sigma$ . The MHA update should be performed separately for each Gaussian. The degrees of freedom of the jumping kernel,  $\nu_k$ , should be chosen such that  $\sim 15\text{--}40\%$  of the MHA jumps are accepted.

If there are any bounds on  $\Sigma_k$  incorporated into the prior distribution, then values of  $\Sigma_k$  that fall outside of this range should automatically be rejected. Methods for simulating from the Wishart distribution, as well as the functional form of the Wishart distribution, are given in § C.

5. Draw a proposal for the prior parameter  $\mu_0$  as  $\hat{\mu}_0 \sim N_2(\tilde{\mu}_0, V_0)$ . The acceptance ratio only depends on the prior distribution and is

$$r_0 = \left[ \prod_{k=1}^K \frac{\text{Cauchy}_2(\mu_k|\hat{\mu}_0, T)}{\text{Cauchy}_2(\mu_k|\tilde{\mu}_0, T)} \right] \left[ \frac{\int_{\log L_{low}}^{\log L_{high}} \int_{\log z_{low}}^{\log z_{high}} \text{Cauchy}_2(\mu_k|\tilde{\mu}_0, T) d\mu_k}{\int_{\log L_{low}}^{\log L_{high}} \int_{\log z_{low}}^{\log z_{high}} \text{Cauchy}_2(\mu_k|\hat{\mu}_0, T) d\mu_k} \right]^K. \quad (29)$$

Here,  $T$  is given by Equation (19) and the integrals are needed because of the prior constraints on  $\mu$ . If  $r_0 \geq 1$  then set  $\tilde{\mu}_0 = \hat{\mu}_0$ , otherwise set  $\tilde{\mu}_0 = \hat{\mu}_0$  with probability  $r_0$ . We have found a good choice for  $V_0$  to be the sample covariance matrix of  $\tilde{\mu}$ .

6. Finally, update the value of  $A$ , the common scale matrix. Because we can approximately calculate the conditional distribution of  $A$ , given  $\Sigma$ , we can directly simulate from  $p(A|\Sigma)$ . Directly simulating from the conditional distributions is referred to as a Gibbs sampler. We perform a Gibbs update to draw a new value of  $\hat{A}$ :

$$\hat{A} \sim \text{Wishart}_{\nu_A}(S) \quad (30)$$

$$\nu_A = K + 3 \quad (31)$$

$$S = \left( \sum_{k=1}^K \tilde{\Sigma}_k^{-1} \right)^{-1}. \quad (32)$$

For the Gibbs sampler update, we do not need to calculate an acceptance ratio, and every value of  $\hat{A}$  is accepted:  $\tilde{A} = \hat{A}$ . If there are any prior bounds set on  $\Sigma$ , then this is technically only an approximate Gibbs update, as

it ignores the constraint on  $\Sigma$ . A true MHA update would account for the constraint on  $\Sigma$  by renormalizing the conditional distribution appropriately; however, this involves a triple integral that is expensive to compute. If there are prior bounds on  $\Sigma$ , then Equation (30) is approximately correct, and ignoring the normalization in  $p(A|\Sigma)$  does not have any effect on our results.

Steps 2–6 are repeated until the MCMC converges, where one saves the values of  $\tilde{\theta}$  at each iteration. After convergence, the MCMC is stopped, and the values of  $\tilde{\theta}$  may be treated as a random draw from the marginal posterior distribution of  $\theta$ ,  $p(\theta|\log L_{obs}, \log z_{obs})$ . Techniques for monitoring convergence of the Markov Chains are described in Gelman et al. (2004). If one wishes to assume a uniform prior on  $\mu$  and  $\Sigma$ , constrained within some set range, instead of the prior we suggest in § 4.1, then only steps 2–4 need to be performed. Given the values of  $\theta$  obtained from the MCMC, one can then draw values of  $N$  from the negative binomial density (cf. Eq.[13]). In § C we describe how to simulate random variables from a negative binomial distribution. The speed of our MHA algorithm depends on the sample size and the programming language. As a rough guide, on a modern computer our MHA can take a couple of hours to converge for sample sizes of  $\sim 1000$ , and our MHA can take as long as a day or two to converge for sample sizes  $\sim 10^4$ .

When performing the MCMC it is necessary to perform a ‘burn-in’ stage, after which the Markov chains have approximately converged to the posterior distribution. The values of  $\theta$  from the MCMC during the burn-in stage are discarded, and thus only the values of  $\theta$  obtained after the burn-in stage are used in the analysis. We have found it useful to perform  $\sim 10^4$  iterations of burn-in, although this probably represents a conservative number. In addition, the parameters for the MHA jumping distributions should be tuned during the burn-in stage. In particular, the parameters  $\Sigma_\alpha, \sigma_{\sigma_l}^2, c_\pi, \Sigma_{\mu,k}$ , and  $\nu_k$  should be varied within the burn-in stage to make the MHA more efficient and have an acceptance rate of  $\sim 0.15$ – $0.4$  (Gelman, Roberts, & Gilks 1995). These jumping distribution parameters cannot be changed after the burn-in stage. Jasra et al. (2005) and Neal (1996) described additional complications and considerations developing MHAs for mixture models.

Some post processing of the Markov chains is necessary. This is because some chains can get ‘stuck’ wandering in regions far below flux limit, likely in the presence of a local maximum in the posterior. While such chains will eventually converge and mix with the other chains, they do not always do so within the finite number of iterations used when running the random walk MHA. We argued in § 4.1 that the Gaussian centroids should be limited to some specified range in  $L$  and  $z$  to prevent the chains from getting stuck. However, this is only a partial fix, as the minimum luminosity for the Gaussian function means may be significantly fainter than the flux limit at a given redshift,  $L_{lim}(z)$ ; i.e.,  $\mu_l \geq \log L_{low}$  and  $L_{low} < L_{lim}(z)$ . In general, we have found that divergent chains are easy to spot. Because the divergent chains usually get stuck in regions far below the flux limit, they correspond to luminosity functions with implied extremely low detection probabilities, i.e.,  $p(I=1|\theta) \ll 1$ . As a result, the random draws of  $N$  from the posterior for these chains tend to have values that are too high and far removed from the rest of the posterior distribution of  $N$ . The divergent chains are therefore easily found and removed by inspecting a histogram of  $\log N$ . In fact, we have found that the divergent chains often become too large for the long integer format used in our computer routines, and therefore are returned as negative numbers. Because negative values of  $N$  are unphysical, it is easy to simply remove such chains from the analysis.

Having obtained random draws of  $N$  and  $\theta$  from  $p(\theta, N|\log L_{obs}, \log z_{obs})$ , one can then use these values to calculate an estimate of  $\phi(L, z)$ , and its corresponding uncertainty. This is done by inserting the MCMC values of  $\theta$  and  $N$  directly into Equation (18). The posterior distribution of  $\phi(L, z)$  can be estimated for any value of  $L$  and  $z$  by plotting a histogram of the values of  $\phi(L, z)$  obtained from the MCMC values of  $\theta$  and  $N$ . In § 6, we illustrate in more detail how to use the MHA results to perform statistical inference on the LF.

## 6. APPLICATION TO SIMULATED DATA

As an illustration of the effectiveness of our method, we applied it to a simulated data set. We construct a simulated sample, and then recover the luminosity function based on our mixture of Gaussian functions model. We assume the effective survey area and selection function reported for the DR3 quasar sample (Richards et al. 2006).

### 6.1. Construction of the Simulated Sample

We first drew a random value of  $N_\Omega$  quasars from a binomial distribution with probability of success  $\Omega/4\pi = 0.0393$  and number of trials  $N = 3 \times 10^5$ . Here,  $\Omega = 1622 \text{ deg}^2$  is the effective sky area for our simulated survey, and we chose the total number of quasars to be  $N = 3 \times 10^5$  in order to ultimately produce a value of  $n \sim 1300$  observed sources, after accounting for the SDSS selection function. This first step of drawing from a binomial distribution simulates a subset of  $N_\Omega \sim 1.2 \times 10^4$  sources from  $N$  total sources randomly falling within an area  $\Omega$  on the sky. For simplicity, in this simulation we ignore the effect of obscuration on the observed quasar population. While our choice of  $N = 3 \times 10^5$  produces a much smaller sample than the actual sample of  $n \sim 1.5 \times 10^4$  quasars from the SDSS DR3 luminosity function work (Richards et al. 2006), we chose to work with this smaller sample to illustrate the effectiveness of our method on more moderate sample sizes.

For each of these  $N_\Omega \sim 1.2 \times 10^4$  sources, we simulated values of  $L$  and  $z$ . We first simulated values of  $\log z$  from a marginal distribution of the form

$$f(\log z) = \frac{4\Gamma(a+b)}{\Gamma(a)\Gamma(b)} \frac{\exp(a\zeta^*)}{(1 + \exp(\zeta^*))^{a+b}}, \quad (33)$$

where  $\zeta^* = 4(\log z - 0.4)$ . The parameters  $a = 1.25$  and  $b = 2.5$  were chosen to give an observed redshift distribution

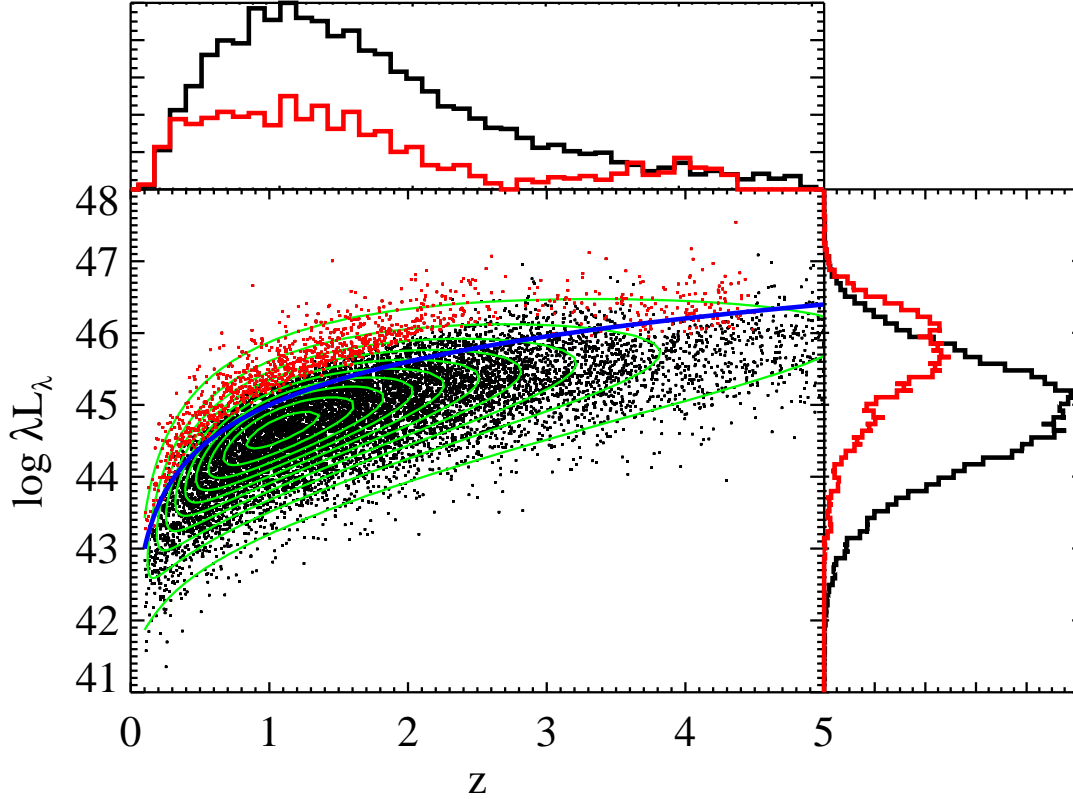


FIG. 5.— The distribution of  $L$  and  $z$  for the simulated sample described in § 6.1. Red dots denote sources included in the sample, black dots denote sources not included in the sample, the blue line denotes  $L^*$  as a function of  $z$ , and the green contours display the 2-d luminosity function. Also shown are histograms of the marginal distributions of  $\log L$  and  $z$ , for all simulated objects (black histogram) and only the detected ones (red histogram). For clarity, the histogram of the detected sources has been forced to peak at a value equal to half of the peak of the histogram of all objects.

similar to that seen for SDSS DR3 quasars (e.g., Richards et al. 2006). Values of  $\log z$  are easily drawn from Equation (33) by first drawing  $x^* \sim \text{Beta}(a, b)$ , and then setting  $\log z = \text{logit}(x^*)/4 + 0.4$ ; here,  $\text{Beta}(a, b)$  is a beta probability density, and  $\text{logit}(x) = \ln(x/(1-x))$  is the logit function.

For each simulated value of  $z$ , we simulated a value of  $L$  using a similar functional form. The conditional distribution of  $\log L$  given  $z$  is

$$f(\log L|z) = \frac{\Gamma(\alpha(z) + \beta(z))}{\Gamma(\alpha(z))\Gamma(\beta(z))} \frac{(L/L^*(z))^{\alpha(z)/\ln 10}}{[1 + (L/L^*(z))^{1/\ln 10}]^{\alpha(z) + \beta(z)}} \quad (34)$$

$$\alpha(z) = 6 + \log z \quad (35)$$

$$\beta(z) = 9 + 2 \log z \quad (36)$$

$$L^*(z) = 10^{45} z^2, \quad (37)$$

where  $L^*(z)$  approximately marks the location of the peak in  $f(\log L|z)$ ,  $t(z)$  is the age of the universe in Gyr at redshift  $z$ ,  $\alpha(z)$  is the slope of  $\log f(\log L|z)$  for  $L \lesssim L^*(z)$ , and  $\beta(z)$  is the slope of  $\log f(\log L|z)$  for  $L \gtrsim L^*(z)$ . In this simulated ‘universe’, both the peak and logarithmic slopes of the LF evolve. The form of the luminosity function assumed by Equation (34) is similar to the double power-law form commonly used in the quasar LF literature, but has a more gradual transition between the two limiting slopes.

After using Equations (33) and (34) to generate random values of  $L$  and  $z$ , we simulated the effects at a selection function. We randomly kept each source for  $z < 4.5$ , where the probability of including a source given its luminosity and redshift was taken to be the SDSS DR3 Quasar selection function, as reported by Richards et al. (2006). After running our simulated sample through the selection function, we were left with a sample of  $n \sim 1300$  sources. Therefore, our simulated survey is only able to detect  $\sim 0.4\%$  of the  $N = 3 \times 10^5$  total quasars in our simulated ‘universe’. The distributions of  $L$  and  $z$  are shown in Figure 5 for both the detected sources and the full sample. As can be seen, the majority of sources are missed by our simulated survey.

The joint probability distribution of  $L$  and  $z$  is  $f(L, z) = f(L|z)f(z)$ , and therefore Equations (33) and (34) imply



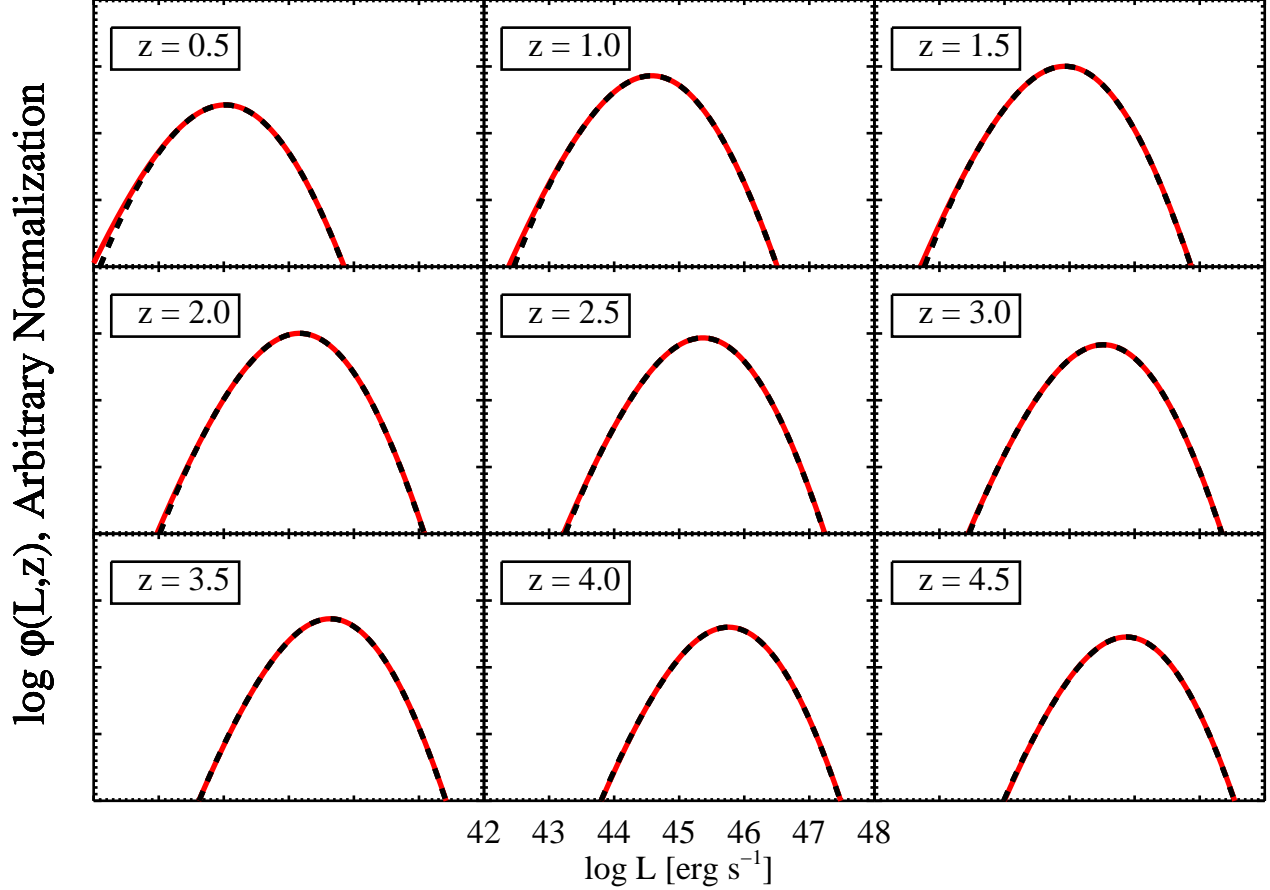


FIG. 6.— The true LF (solid red line) at several values of  $z$ , and the best  $K = 4$  Gaussian function fit (dashed black line). In this case, approximating the LF with four 2-dimensional Gaussian functions provides an excellent fit.

that the true LF for our simulated sample is

$$\phi_0(L, z) = \frac{N}{zL(\ln 10)^2} \left( \frac{dV}{dz} \right)^{-1} f(\log L|z) f(\log z) \quad (38)$$

Figure 6 shows  $\phi_0(L, z)$  at several redshifts. Also shown in Figure 6 is the best fit for a mixture of  $K = 4$  Gaussian functions. Despite the fact that  $\phi_0(L, z)$  has a rather complicated parametric form, a mixture of four Gaussian functions is sufficient to achieve an excellent approximation to  $\phi_0(L, z)$ ; in fact, the mixture of four Gaussian functions is indistinguishable from the true LF.

### 6.2. Performing Statistical Inference on the LF with the MCMC Output

We performed the MHA algorithm described in § 5 to obtain random draws from the posterior probability distribution for our this simulated sample, assuming the Gaussian mixture model described in § 4. We performed  $10^4$  iterations of burn-in, and then ran the Markov chains for  $3 \times 10^4$  more iterations. We ran 20 chains simultaneously in order to monitor convergence (e.g., see Gelman et al. 2004) and explore possible multimodality in the posterior. We saved the values of  $\theta$  for the Markov chains after the initial  $10^4$  burn-in iterations, and, after removing divergent chains with  $N < 0$  we were left with  $\sim 8 \times 10^4$  random draws from the posterior distribution,  $p(\theta, N|L_{obs}, z_{obs})$ .

The output from the MCMC can be used to perform statistical inference on the LF. Denote the  $T \sim 8 \times 10^4$  random draws of  $\theta$  and  $N$  obtained via the MHA as  $\theta^1, \dots, \theta^T$  and  $N^1, \dots, N^T$ , respectively. The individual values of  $(\theta^t, N^t)$  can then be used to construct histograms as estimates of the posterior distribution for each parameter. For each random draw of  $\theta$  and  $N$ , we can also calculate a random draw of  $\phi(L, z)$  from its posterior distribution. In particular, the  $t^{\text{th}}$  random draw of the LF under the mixture of normals model, denoted as  $\phi^t(L, z)$ , is calculated by inserting  $\theta^t$  and  $N^t$  into Equation (18). The  $T$  values of  $\phi^t(L, z)$  can then be used to estimate the posterior distribution of  $\phi(L, z)$  for any given value of  $L$  and  $z$ . Furthermore, random draws from the posterior for quantities that are computed directly from the LF, such as the location of its peak as a function of  $z$ , are obtained simply by computing the quantity of interest from each of the  $T$  values of  $\phi^t(L, z)$ .

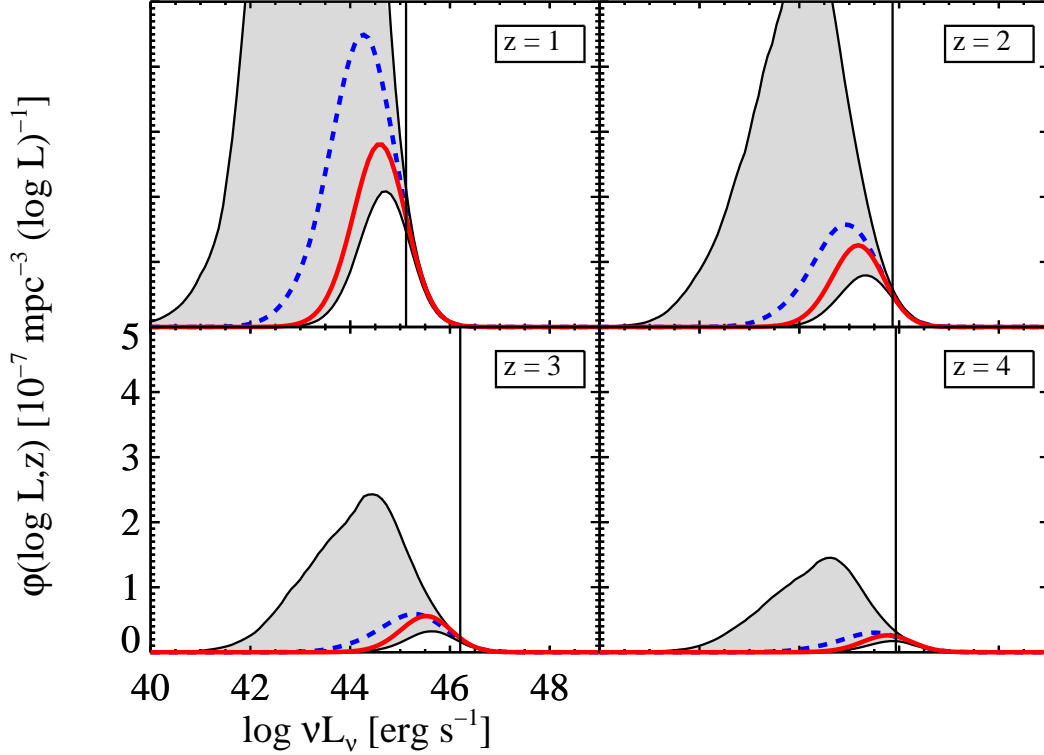


FIG. 7.— The true LF (solid red line) at several redshifts for the simulated sample described in § 6.1. The axis labels are the same for all panels, but for clarity we only label the bottom left panel. Also shown is the posterior median estimate of the LF based on the mixture of Gaussian functions model (dashed blue line), the region containing 90% of the posterior probability (shaded region). The Bayesian mixture of Gaussian functions model is able to accurately constrain the LF, even below the survey detection limit.

In Figures 7 and 8 we show  $\phi(\log L, z)$  at several different redshifts, on both a linear scale and a logarithmic scale. In general, we find it easier to work with  $\phi(\log L, z) = \ln 10 L \phi(L, z)$ , as  $\phi(\log L, z)$  can span several orders of magnitude in  $L$ . Figures 7 and 8 show the true value of the LF,  $\phi_0(\log L, z)$ , the best-fit estimate of  $\phi(\log L, z)$  based on the mixture of Gaussian functions model, and the regions containing 90% of the posterior probability. Here, as well as throughout this work, we will consider the posterior median of any quantity to be the ‘best-fit’ for that quantity. In addition, in this work we will report errors at the 90% level, and therefore the regions containing 90% of the posterior probability can be loosely interpreted as asymmetric error bars of length  $\approx 1.65\sigma$ . The region containing 90% of the probability for  $\phi(\log L, z)$  is easily estimated from the MCMC output by finding the values of  $t_1$  and  $t_2$  such that 90% of the values of  $\phi^1(\log L, z), \dots, \phi^T(\log L, z)$  have  $\phi^{t_1}(\log L, z) < \phi^t(\log L, z) < \phi^{t_2}(\log L, z)$ . As can be seen, the true value of  $\phi(\log L, z)$  is contained within the 90% probability region for all almost values of  $L$ , even those below the survey detection limit.

Figure 9 compares the true integrated  $z < 6$  number distribution of  $\log L$ ,  $n(\log L, z < 6)$ , with the mixture of Gaussian functions estimate. The quantity  $n(\log L, z < 6)d\log L$  gives the number of quasars at  $z < 6$  with black hole masses between  $\log L$  and  $\log L + d\log L$ . It is calculated as

$$n(\log L, z < 6) = \int_0^6 \phi(\log L, z) \left( \frac{dV}{dz} \right) dz, \quad (39)$$

which, for the mixture of normals model, is

$$n(\log L, z < z_0) = N \sum_{k=1}^K \pi_k N(\log L | \mu_{l,k}, \sigma_{l,k}^2) \Phi \left[ \frac{\log z_0 - E(\log z | L, k)}{\sqrt{\text{Var}(\log z | L, k)}} \right] \quad (40)$$

$$E(\log z | L, k) = \mu_{z,k} + \frac{\sigma_{lz,k}}{\sigma_{z,k}^2} (\log L - \mu_{l,k}) \quad (41)$$

$$\text{Var}(\log z | L, k) = \sigma_{z,k}^2 - \frac{\sigma_{lz,k}^2}{\sigma_{z,k}^2}. \quad (42)$$

Here,  $\Phi(\cdot)$  is the cumulative distribution function for the standard normal density. Similar to Figures 7 and 8, the

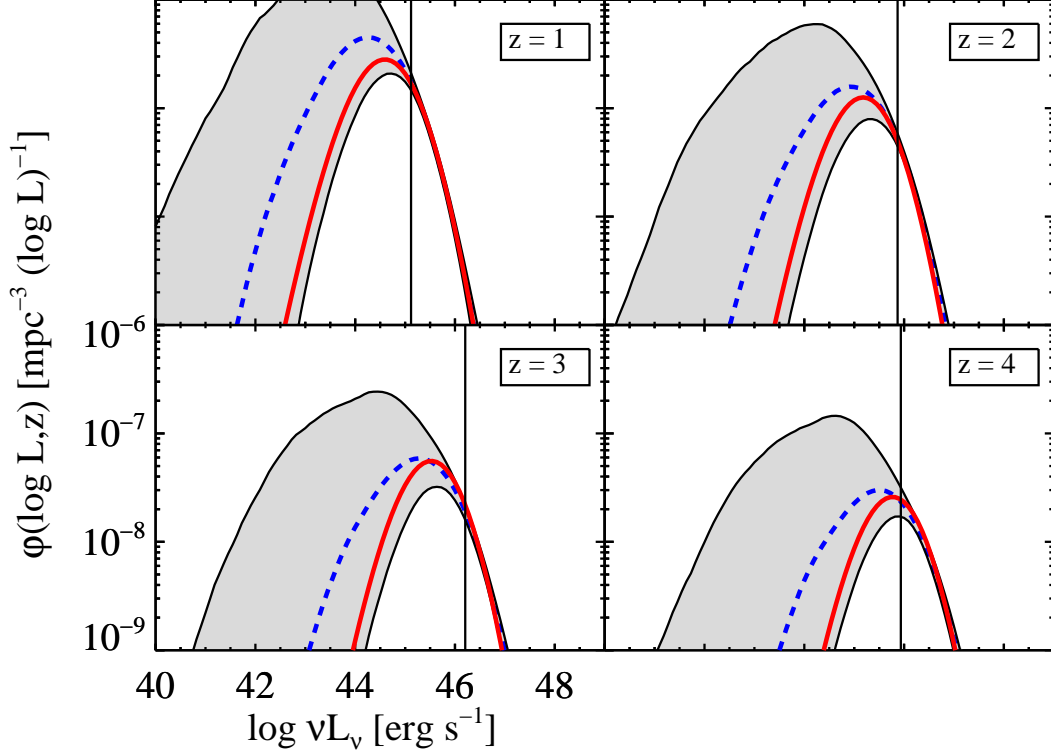


FIG. 8.— Same as Figure 7, but shown with a logarithmic stretch.

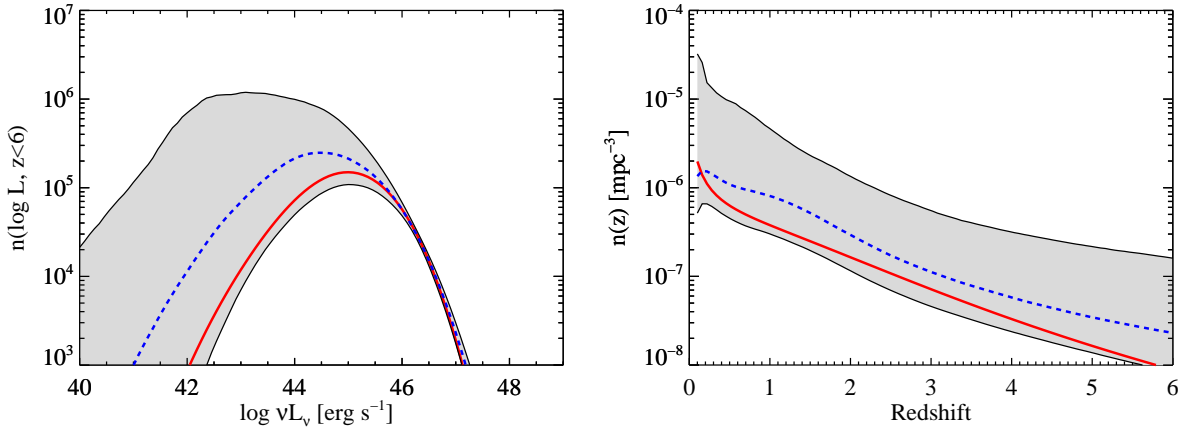


FIG. 9.— The integrated  $z < 6$  quasar number density (number per  $\log L$  interval, left) and the quasar comoving quasar number density as a function of  $z$  (number per  $\text{mpc}^3$ , right) for the simulated sample described in § 6.1. As with Figure 7, the solid red line denotes the true value for the simulation, the dashed blue line denotes the posterior median for the mixture of Gaussian functions model, and the shaded region contain 90% of the posterior probability. The posterior median provides a good fit to the true values, and the uncertainties derived from the MCMC algorithm based on the Gaussian mixture model are able to accurately constrain the true values of these quantities, despite the flux limit.

true value of  $n(\log L, z < 6)$  is contained within the 90% probability region for all values of  $L$ , even those below the survey detection limit.

In addition, in Figure 9 we show the comoving number density of broad line AGN as a function of redshift,  $n(z)$ . This is obtained by integrating  $\phi(L, z)$  over all possible values of  $L$ . For the mixture of normals model, this becomes

$$n(z) = N \left( \frac{dV}{dz} \right)^{-1} \sum_{k=1}^K \pi_k p(z|k), \quad (43)$$

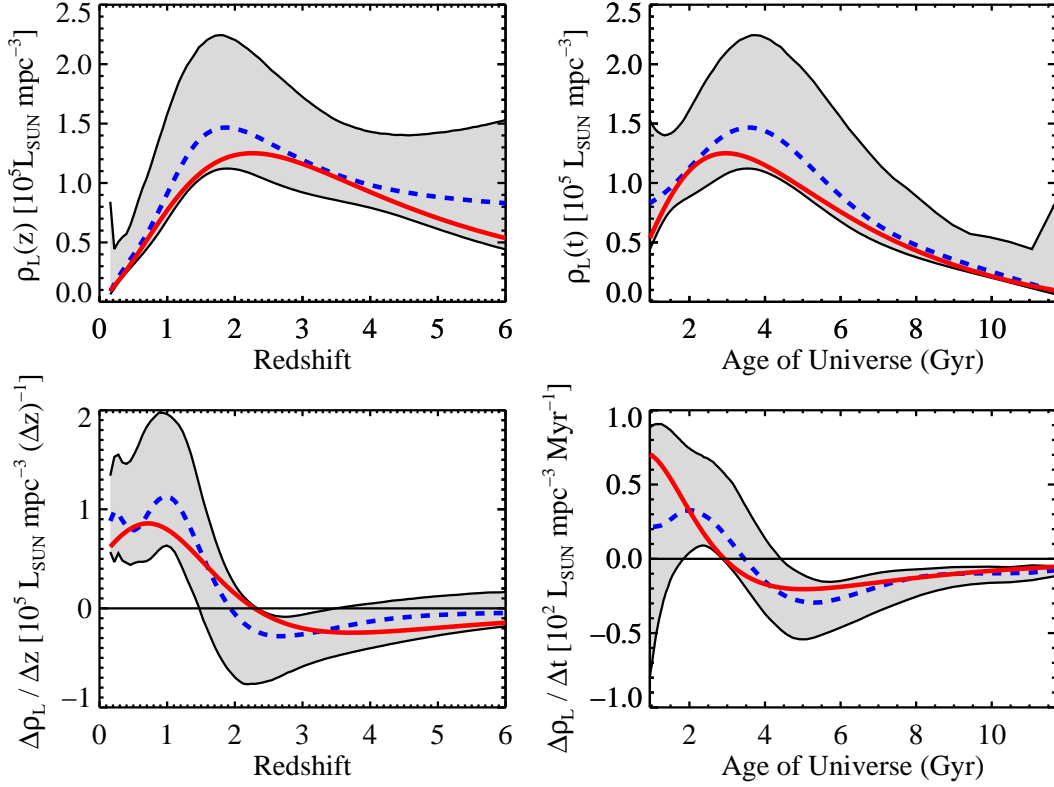


FIG. 10.— Comoving quasar luminosity density (top two panels) and its derivative (bottom two panels), shown as a function of redshift (left two panels) and cosmic age (right two panels) for the simulated sample described in § 6.1. The plotting symbols are the same as in Figure 9. As in the previous figures, the Gaussian mixture model is able to provide an accurate fit to the true values of  $\rho_L(z)$ , and the bayesian MCMC approach is able to provide accurate constraints on  $\rho_L(z)$  and  $d\rho_L/dz$ , despite the fact that the integral used for calculating these quantities extends below the survey detection limit.

where the marginal distribution of  $z|k$  is

$$p(z|k) = \frac{1}{z \ln 10 \sqrt{2\pi\sigma_{z,k}^2}} \exp \left\{ -\frac{1}{2} \left( \frac{\log z - \mu_{z,k}}{\sigma_{z,k}} \right)^2 \right\}. \quad (44)$$

As before, the true value of  $n(z)$  is contained within the 90% probability region, despite the fact that the integration extends over *all*  $L$ , even those below the detection limit. The wider confidence regions reflect additional uncertainty in  $n(z)$  resulting from integration over those  $L$  below the detection limit. In particular, the term  $dV/dz$  becomes small at low redshift, making the estimate of  $n(z)$  more unstable as  $z \rightarrow 0$ , and thus inflating the uncertainties at low  $z$ .

Two other potentially useful quantities are the comoving luminosity density for quasars,  $\rho_L(z)$ , and its derivative. The comoving quasar luminosity density is given by  $\rho_L(z) = \int_0^\infty L \phi(L, z) dL$ . For the mixture of Gaussian functions model it may be shown that

$$\rho_L(z) = N \left( \frac{dV}{dz} \right)^{-1} \sum_{k=1}^K \pi_k p(z|k) \exp \left\{ \ln 10 E(\log L|z, k) + \frac{(\ln 10)^2}{2} \text{Var}(\log L|z, k) \right\} \quad (45)$$

$$E(\log L|z, k) = \mu_{l,k} + \frac{\sigma_{lz,k}}{\sigma_{z,k}^2} (\log z - \mu_{z,k}) \quad (46)$$

$$\text{Var}(\log L|z, k) = \sigma_{l,k}^2 - \frac{\sigma_{lz,k}^2}{\sigma_{z,k}^2}, \quad (47)$$

where  $p(z|k)$  is given by Equation (44). We calculate the derivative of  $\rho_L(z)$  numerically. Figure 10 compares the true values of  $\rho_L(z)$  and its derivative with the posterior distribution for  $\rho_L(z)$  inferred from the mixture model, both as a function of  $z$  and the age of the universe at redshift  $z$ ,  $t(z)$ . Comparison with Figure 9 reveals that the comoving quasar luminosity density,  $\rho_L(z)$ , is a better constrained quantity than the comoving quasar number density,  $n(z)$ . Furthermore,  $n(z)$  appears to peak much later than  $\rho_L(z)$ . In addition, we can correctly infer that the comoving quasar luminosity density reaches its point of fastest growth at  $t(z) \sim 2$  Gyr, and its point of fastest decline at  $t(z) \sim 5$  Gyr.

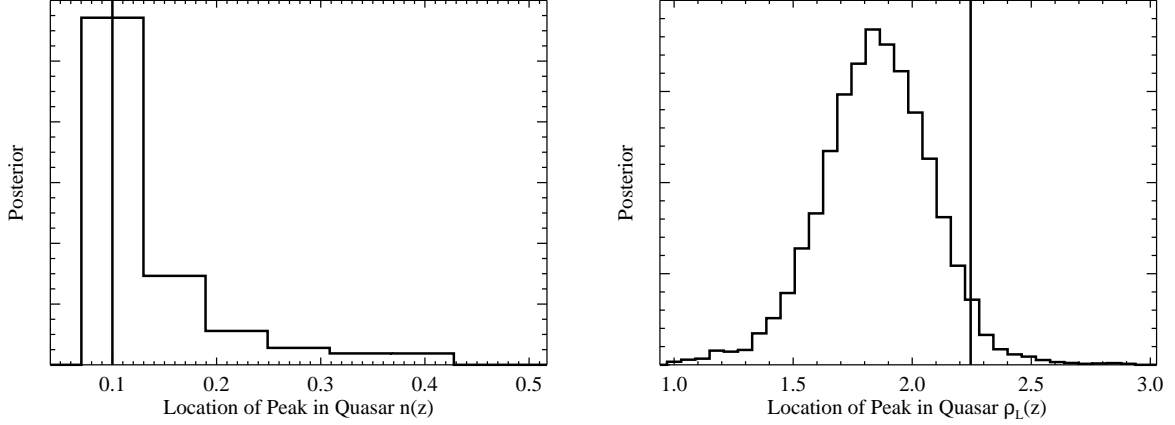


FIG. 11.— Posterior distribution for the redshift location of the peak in the comoving number density of quasars (left) and the peak in the comoving quasar luminosity density (right) for the simulated sample described in § 6.1. For clarity we only show the posterior distribution for the peak in  $n(z)$  at  $z > 0.5$ , since values of the peak at  $z < 0.5$  arise because the term  $(dV/dz)^{-1}$  becomes very large at low  $z$ . The vertical lines denote the true values. The posterior distribution inferred from the MCMC output is able to accurately constrain the true values of the argumentative maximum in  $n(z)$  and  $\rho_L(z)$ .

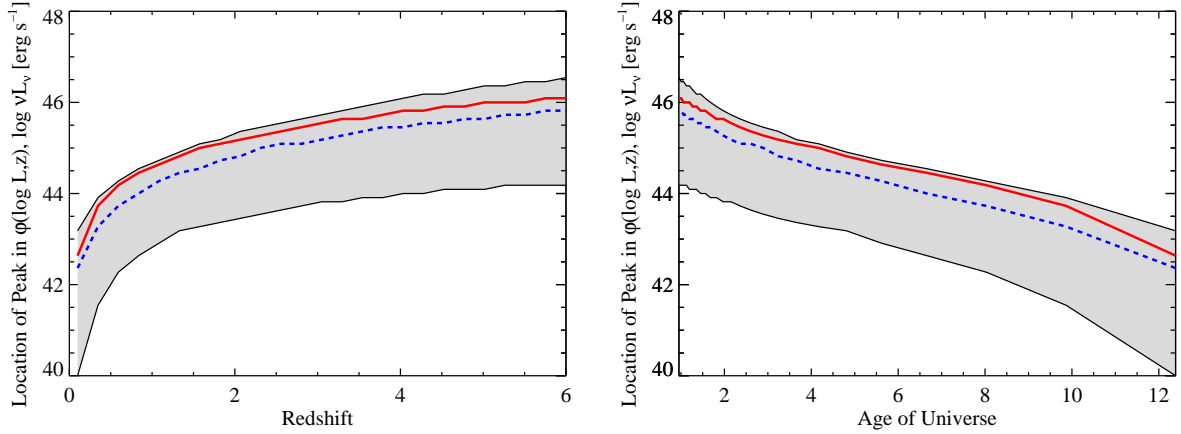


FIG. 12.— Location of the peak in the LF as a function of  $z$  (left) and cosmic age (right) for the simulated sample described in § 6.1. The plot symbols are the same as in Figure 9. In general the posterior median of the Gaussian mixture model provides a good estimate of the true peak locations, although the uncertainty is high due to the survey flux limit. However, it is clear from these plots that the location of the peak in  $\phi(L, z)$  evolves.

Figure 11 quantifies the suggestion that  $n(z)$  peaks later than  $\rho_L(z)$  by displaying the posterior distribution for the location of the respective peaks in  $n(z)$  and  $\rho_L(z)$ . We can still constrain the peak in  $n(z)$  to be at  $z \lesssim 0.5$ . In contrast, the location of the peak in  $\rho_L(z)$  is constrained to occur earlier at  $1 \lesssim z \lesssim 3$ . This is a consequence of the fact that while there were more quasars per comoving volume element in our simulated universe at  $z \lesssim 0.5$ , their luminosities were much higher at higher redshift. This evolution in characteristic  $L$  is quantified in Figure 12, which summarizes the posterior distribution for the location of the peak in  $\phi(\log L, z)$  as a function of redshift and  $t(z)$ . As can be seen, the location of the peak in the LF shows a clear trend of increasing ‘characteristic’  $L$  with increasing  $z$ , although there is considerable uncertainty on the actual value of the location of the peak.

### 6.3. Using the MCMC Output to Evaluate the LF Fit

Throughout this section we have been analyzing the MCMC results by comparing to the true LF. However, in practice we do not have access to the true LF, and thus a method is needed for assessing the quality of the fit. The statistical model may be checked using a technique known as posterior predictive checking (e.g., Rubin 1981, 1984; Gelman, Meng, & Stern 1998). Here, the basic idea is to use each of the MCMC outputs to simulate a new random observed data set. The distributions of the simulated observed data sets are then compared to the true observed data in order to assess whether the statistical model gives an accurate representation of the observed data. It is important to construct simulated data sets for each of the MCMC draws in order to incorporate our uncertainty in the model parameters.

For each value of  $N^t$  and  $\theta^t$  obtained from the MCMC output, a simulated data set of  $(l_{obs}^t, z_{obs}^t)$  may be obtained through a similar procedure to that described in § 6.1. First, one draws a value of  $N_{\Omega}^t$  from a binomial distribution

with  $N^t$  trials and probability of ‘success’  $p = \Omega/4\pi$ . Then, one draws  $N_\Omega^t$  values of  $L^t$  and  $z^t$  from  $p(L, z|\theta^t)$ .

For our model,  $p(\log L, \log z|\theta^t)$  is a mixture of normal densities, and one needs to employ a two-step process in order to simulate a random value from  $p(\log L, \log z|\theta^t)$ . First, one needs to randomly assign the  $i^{\text{th}}$  data point to one of the Gaussian distributions. Since  $\pi_k$  gives the probability that a data point will be drawn from the  $k^{\text{th}}$  Gaussian distribution, one first needs to simulate a random vector  $\mathbf{G}_i^t$  from a multinomial distribution with one trial and probability of success for the  $k^{\text{th}}$  class  $\pi_k^t$ ; i.e., first draw  $\mathbf{G}_i^t \sim \text{Multinom}(1, \pi_1^t, \dots, \pi_K^t)$ . The vector  $\mathbf{G}_i^t$  gives the class membership for the  $i^{\text{th}}$  data point, where  $G_{ik}^t = 1$  if the  $i^{\text{th}}$  data point comes from the  $k^{\text{th}}$  Gaussian, and  $G_{ij}^t = 0$  if  $j \neq k$ . Then, given  $G_{ik}^t = 1$ , one then simulates a value of  $(\log L_i^t, \log z_i^t)$  from a 2-dimensional Gaussian distribution with mean  $\mu_k^t$  and covariance matrix  $\Sigma_k^t$ . This is repeated for all  $N_\Omega^t$  sources, leaving one with a random sample  $(\log L^t, \log z^t) \sim p(\log L, \log z|\theta^t)$ .

A random draw from  $\text{Multinom}(1, \pi_1, \dots, \pi_K)$ , may be obtained as a sequence of binomial random draws. First, draw  $n'_1 \sim \text{Binomial}(1, \pi_1)$ . If  $n'_1 = 1$ , then assign the data point to the first Gaussian distribution, i.e., set  $G_{i1} = 1$ . If  $n'_1 = 0$ , then draw  $n'_2 \sim \text{Binomial}(1, \pi_2 / \sum_{k=2}^K \pi_k)$ . If  $n'_2 = 1$ , then assign the data point to the second Gaussian distribution, i.e., set  $G_{i2} = 1$ . If  $n'_2 = 0$ , then the process is repeated for the remaining Gaussian distribution as follows. For  $j = 3, \dots, K-1$ , sequentially draw  $n'_j \sim \text{Binomial}(1, \pi_j / \sum_{k=j}^K \pi_k)$ . If at any time  $n'_j = 1$ , then stop the process and assign the data point to the  $j^{\text{th}}$  Gaussian distribution. Otherwise, if none of the  $n'_j = 1$ , then assign the data point to the  $K^{\text{th}}$  Gaussian distribution.

Once one obtains a random draw of  $(L^t, z^t)$ , randomly ‘observe’ these sources, where the probability of including a source given  $L_i^t$  and  $z_i^t$  is given by the selection function. This will leave one with a simulated observed data set,  $(L_{obs}^t, z_{obs}^t)$ . This process is repeated for all  $T$  values of  $N^t$  and  $\theta^t$  obtained from the MCMC output, leaving one with  $T$  simulated data sets of  $(L_{obs}^t, z_{obs}^t)$ . One can then compare the distribution of the simulated data sets with the true values of  $L_{obs}$ , and  $z_{obs}$  to test the statistical model for any inconsistencies.

In Figure 13 we show histograms for the true observed distributions of  $z$  and  $\log L$ . These histograms are compared with the posterior median of the distributions based on the mixture of Gaussian functions model, as well as error bars containing 90% of the simulated values. Also shown is a plot comparing the true values of the maximum of  $L_{obs}$  as a function of  $z$  with those based on  $L_{obs}^t$  and  $z_{obs}^t$ . As can be seen, the distributions of the observed data assuming the mixture of Gaussian functions model are consistent with the true distributions of the observed data, and therefore there is no reason to reject the mixture model as providing a poor fit.

## 7. SUMMARY

We have derived the observed data likelihood function which relates the quasar LF to the observed distribution of redshifts, luminosities. This likelihood function is then used in a Bayesian approach to estimating the LF, where the LF is approximated as a mixture of Gaussian functions. Because much of this work was mathematically technical, we summarize the important points here.

- Equation 6 gives the likelihood function for an assumed parametric luminosity function. This likelihood function differs from the Poisson likelihood commonly used in the LF literature because it correctly models the sample size as a binomial random variable, whereas the Poisson likelihood approximates the sample size as a Poisson random variable. In practice, the difference in the maximum-likelihood estimates obtained from the two likelihood functions do not seem to be significantly different so long as the probability of including a source in a survey is small.
- The product of Equations (12) and (13) is the joint posterior probability distribution of the LF, given the observed data. These equations may be used to perform Bayesian inference on the LF, after assuming a prior distribution on the LF parameters. Bayesian inference is often most easily performed by simulating random variables drawn from the posterior probability distribution. These random draws may be used to estimate the posterior distribution for the LF, as well as to estimate the posterior distribution for any quantities calculated from the LF. The posterior distribution provides statistically accurate uncertainties on the LF and related quantities, even when the sample size is small and one is including information below the survey detection limits. In contrast, confidence intervals derived from bootstrapping the maximum-likelihood estimate can be too small.
- We describe a flexible model for the LF, where the LF is modeled as a mixture of Gaussian functions. Equation (17) describes the probability distribution of  $\log L$  and  $\log z$  under the mixture of Gaussian functions model, and (18) describes the LF under the mixture of Gaussian functions model. Equation (21) gives our prior distribution for the Gaussian function parameters. The marginal posterior distribution of the mixture model parameters is given by Equation (22), the conditional posterior distribution of  $N$  at a given  $\theta$  is given by Equation (13), and the complete joint posterior distribution is the product of Equations (22) and (13).
- We describe in § 5 a Metropolis-Hastings algorithm for obtaining random draws from the posterior distribution for the LF assuming a Schechter function or mixture of Gaussian functions model. In § 6, we use a simulated sample, modeled after the SDSS DR3 Quasar Catalog, to illustrate the effectiveness of our statistical method,

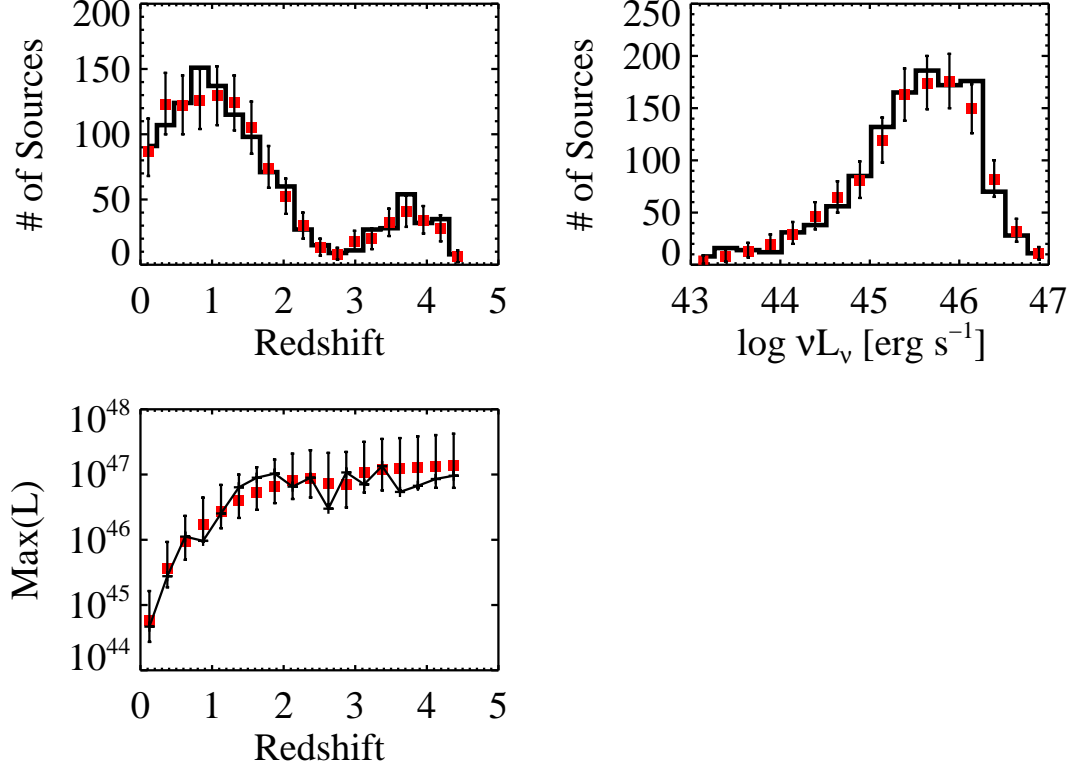


FIG. 13.— Posterior predictive check for the Gaussian mixture model (see § 6.3). The histograms show the actual distributions of  $L_{obs}$  and  $z_{obs}$ , the red squares denote the posterior medians for the number of sources in each respective bin, and the error bars contain the inner 90% of the histogram values for the samples simulated from the posterior. Also shown is a plot of the maximum observed luminosity as a function of  $z$  for the simulated samples, the red squares mark the value from the actual sample used in the fit, and the error bars contain 90% of the values simulated from the posterior distribution. The mixture of Gaussian functions model is able to provide an accurate prediction of the observed distribution of luminosity, redshift, and line widths, and thus there is not any evidence to reject it as providing a poor fit.

as well as to give an example on how to use the Metropolis-Hastings output to perform statistical inference on the LF and assess the LF fit.

So long as the mixture of Gaussian functions model is an accurate approximation to the true LF over all luminosities, the uncertainties on the LF, assuming the Gaussian mixture model, are trustworthy because they are calculated directly from the probability distribution of the LF, given the observed data. Statistical inference on the LF below the flux limit can become significantly biased if one assumes an incorrect and restrictive parametric form, as extrapolation errors can become large. In this case, the derived posterior may not contain the true LF because the wrong parametric model was assumed; this type of error is known as model misspecification. For example, consider a case when the true LF is a Schechter function, and one is only able to detect sources brighter than  $L^*$ . If one were to assume a power-law for the LF, extrapolation below the flux limit would be significantly biased. In contrast, the mixture of Gaussian functions model, while incorrect, is flexible enough to accurately approximate the true Schechter function form, thus minimizing extrapolation bias due to model misspecification. Of course, in this example, the most accurate results would be obtained by fitting a Schechter function to the data, since it is the correct parametric form. Therefore, the mixture of Gaussian functions model will not perform as well as assuming the correct parametric model, or at least as well as an alternative parametric model that better approximates the true LF.

Although we have focused on the mixture of Gaussian functions model, the likelihood and posterior distribution are applicable for any parametric form, as illustrated in § 3.2. The observed data likelihood function for the LF is given by Equation (6), and the posterior distribution is given by the product of Equations (12) and (13). Then, one can use Equation (1) to ‘plug-in’ any parametric form of the LF into the appropriate likelihood function and posterior distribution, as was done in Equation (15) for a Schechter function. In addition, the metropolis-hastings algorithm is a general method for obtaining random draws from the posterior, and can be developed for any parametric form of the LF. This therefore allows one to perform Bayesian inference for any variety of parametric models of the LF, and one is not merely limited to the mixture of Gaussian functions model or Schechter function considered in this work.

An IDL computer routine written for performing the Metropolis-Hastings algorithm for the mixture of Gaussian functions model is available on request from B. Kelly.

We acknowledge support from NSF grant AST 03-07384 and a David and Lucile Packard Fellowship in Science and Engineering.

## APPENDIX

### MAXIMUM-LIKELIHOOD VS BAYESIAN INFERENCE

In this section we compare the maximum likelihood approach with the Bayesian approach. We do this for readers who are unfamiliar with some of the more technical aspects of the two approaches, with the hope that the discussion in this section will facilitate interpretation of our results in the main body of the paper.

In maximum-likelihood analysis, one is interested in finding the estimate that maximizes the likelihood function of the data. For a given statistical model, parameterized by  $\theta$ , the likelihood function,  $p(x|\theta)$ , is the probability of observing the data, denoted by  $x$ , as a function of the parameters  $\theta$ . The maximum-likelihood estimate, denoted by  $\hat{\theta}$ , is the value of  $\theta$  that maximizes  $p(x|\theta)$ . Under certain regularity conditions,  $\hat{\theta}$  enjoys a number of useful properties. In particular, as the sample size becomes infinite,  $\hat{\theta}$  becomes an unbiased estimate of  $\theta$ . An unbiased estimator is an estimator with expectation equal to the true value, i.e.,  $E(\hat{\theta}) = \theta_0$ , where  $\theta_0$  is the true value of  $\theta$ . Therefore, on average, an unbiased estimator will give the true value of the parameter to be estimated.

Because the maximum likelihood estimate is a function of the data,  $\hat{\theta}$  has a sampling distribution. The sampling distribution of  $\hat{\theta}$  is the distribution of  $\hat{\theta}$  under repeated sampling from the probability distribution of the data. Under certain regularity conditions, the sampling distribution of  $\hat{\theta}$  is asymptotically normal with covariance matrix equal to the average value of the inverse of the Fisher information matrix,  $I(\theta)$ , evaluated at  $\theta_0$ . The Fisher information matrix is the expected value of the matrix of second derivatives of the log-likelihood, multiplied by  $-1$ . Formally, this result states that as  $n \rightarrow \infty$ , then

$$\hat{\theta} \sim N_p(\theta_0, I^{-1}(\theta_0)), \quad (\text{A1})$$

$$I(\theta) = -E \left( \frac{\partial^2}{\partial \theta^2} \ln p(x|\theta) \right), \quad (\text{A2})$$

where  $p$  is the number of parameters in the model, and the expectation in Equation (A2) is taken with respect to the sampling distribution of  $x$ ,  $p(x|\theta_0)$ . Because we do not know  $\theta_0$ , it is common to estimate  $I^{-1}(\theta_0)$  by  $I^{-1}(\hat{\theta})$ . In addition, it is common to estimate  $I(\theta)$  as the matrix of second derivatives of the log-likelihood of one's data, since the sample average is a consistent estimate for the expectation value. Qualitatively, Equation (A1) states that as the sample size becomes large,  $\hat{\theta}$  approximately follows a normal distribution with mean  $\theta_0$  and covariance matrix  $I^{-1}(\hat{\theta})$ . This fact may be used to construct confidence intervals for  $\theta$ .

While the asymptotic results are useful, it is not always clear how large of a sample is needed until Equation (A1) is approximately true. The maximum likelihood estimate can be slow to converge for models with many parameters, or if most of the data is missing. Within the context of luminosity function estimation, the maximum-likelihood estimate will be slower to converge for surveys with shallower flux limits. In addition, Equation (A1) does not hold if the regularity conditions are not met. In general, this is not a concern, but it is worth noting that the asymptotics do not hold if the true value of  $\theta$  lies on the boundary of the parameter space. For example, in the case of a Schechter luminosity function, if the true value of the shape parameter,  $\alpha$  (see [14]), is  $\alpha_0 = -1$ , then Equation (A1) does not hold, since  $\alpha > -1$ . If  $\alpha_0 \approx -1$ , then Equation (A1) is still valid, but it will take a large sample before the asymptotics are valid, as  $\alpha_0$  lies near the boundary of the parameter space.

In Bayesian analysis, one attempts to estimate the probability distribution of the model parameters,  $\theta$ , given the observed data  $x$ . The probability distribution of  $\theta$  given  $x$  is related to the likelihood function as

$$p(\theta|x) \propto p(x|\theta)p(\theta). \quad (\text{A3})$$

The term  $p(x|\theta)$  is the likelihood function of the data, and the term  $p(\theta)$  is the prior probability distribution of  $\theta$ ; the result,  $p(\theta|x)$  is called the posterior distribution. The prior distribution,  $p(\theta)$ , should convey information known prior to the analysis. In general, the prior distribution should be constructed to ensure that the posterior distribution integrates to one, but to not have a significant effect on the posterior. In particular, the posterior distribution should not be sensitive to the choice of prior distribution, unless the prior distribution is constructed with the purpose of placing constraints on the posterior distribution that are not conveyed by the data. The contribution of the prior to  $p(\theta|x)$  becomes negligible as the sample size becomes large.

From a practical standpoint, the primary difference between the maximum likelihood approach and the Bayesian approach is that the maximum likelihood approach is concerned with calculating a point estimate of  $\theta$ , while the Bayesian approach is concerned with mapping out the distribution of  $\theta$ . The maximum likelihood approach uses an estimate of the sampling distribution of  $\hat{\theta}$  to place constraints on the true value of  $\theta$ . In contrast, the Bayesian approach directly calculates the probability distribution of  $\theta$ , given the observed data, to place constraints on the true value of  $\theta$ . It is illustrative to consider the case when the prior is taken to be uniform over  $\theta$ ; assuming the posterior integrates to one, the posterior is then proportional to the likelihood function,  $p(\theta|x) \propto p(x|\theta)$ . In this case, the goal of maximum likelihood is to calculate an estimate of  $\theta$ , where the estimate is the most probable value of  $\theta$ , given the observed data. Then, confidence intervals on  $\theta$  are derived from the maximum likelihood estimate,  $\hat{\theta}$ , usually by



assuming Equation (A1). In contrast, the Bayesian approach is not concerned with optimizing the likelihood function, but rather is concerned with mapping out the likelihood function. Under the Bayesian approach with a uniform prior, confidence intervals on  $\theta$  are derived directly from likelihood function, and an estimate of  $\theta$  can be defined as, for example, the value of  $\theta$  averaged over the likelihood function. So, the maximum likelihood attempts to obtain the ‘most likely’ value of  $\theta$ , while the Bayesian approach attempts to directly obtain the probability distribution of  $\theta$ , given the observed data. Because the Bayesian approach directly estimates the probability distribution of  $\theta$ , and because it does not rely on any asymptotic results, we consider the Bayesian approach to be preferable for most astronomical applications.

#### DERIVATION OF THE MARGINAL POSTERIOR DISTRIBUTION FOR TRUNCATED DATA

Here, we give a derivation of the posterior probability distribution of  $\theta$ , given by Equation (12). If we assume a uniform prior on  $\log N$ , then this is equivalent to assuming the prior  $p(\theta, N) \propto N^{-1}p(\theta)$ . In this case, the posterior distribution is given by

$$p(\theta, N | L_{obs}, z_{obs}) \propto N^{-1}p(\theta)C_n^N [p(I = 0|\theta)]^{N-n} \prod_{i \in \mathcal{A}_{obs}} p(L_i, z_i | \theta). \quad (B1)$$

The marginal posterior distribution of  $\theta$  is obtained by summing the joint posterior over all possible values of  $N$ . For the choice of prior  $p(\theta, \log N) \propto p(\theta)$ , the marginal posterior of  $\theta$  is

$$p(\theta | L_{obs}, z_{obs}) \propto p(\theta) \left[ \prod_{i \in \mathcal{A}_{obs}} p(L_i, z_i | \theta) \right] \sum_{N=n}^{\infty} N^{-1} C_n^N [p(I = 0|\theta)]^{N-n} \quad (B2)$$

$$\propto p(\theta) [p(I = 1|\theta)]^{-n} \left[ \prod_{i \in \mathcal{A}_{obs}} p(L_i, z_i | \theta) \right] \sum_{N=n}^{\infty} C_{n-1}^{N-1} [p(I = 0|\theta)]^{N-n} [p(I = 1|\theta)]^n, \quad (B3)$$

where we arrived at the second Equation by multiplying and dividing the first Equation by  $p(I = 1|\theta)^n$  and noting that  $C_n^N = C_{n-1}^{N-1}(N/n)$ . The term within the sum is the mathematical expression for a negative binomial distribution as a function of  $N$  (see Eq.[C1]). Because probability distributions must be equal to unity when summed over all possible values, the sum is just equal to one. We therefore arrive at Equation (12) by replacing the summation in Equation (B3) with the value of one.

#### SOME PROBABILITY DISTRIBUTIONS USED IN THIS WORK

In this section of the appendix we briefly describe some probability distribution that we employ, but may be unfamiliar to some astronomers.

##### *Negative Binomial*

The negative binomial distribution is closely related to the binomial distribution. The binomial distribution gives the probability of observing  $n$  ‘successes’, given that there have been  $N$  trials and that the probability of success is  $p$ . In contrast, the negative binomial distribution gives the probability of needing  $N$  trials before observing  $n$  successes, given that the probability of success is  $p$ . Within the context of this work, the binomial distribution gives the probability of detecting  $n$  sources, given that there are  $N$  total sources and that the detection probability is  $p$ . The negative binomial distribution gives the probability that the total number of sources is  $N$ , given that we have detected  $n$  sources and that the detection probability is  $p$ . The negative binomial distribution is given by

$$p(N | n, p) = C_{n-1}^{N-1} p^n (1-p)^{N-n}, \quad N \geq n. \quad (C1)$$

A random draw from the negative binomial distribution with parameters  $n$  and  $p$  may be simulated by first drawing  $n$  random values uniformly distributed on  $[0, 1]$ ,  $u_1, \dots, u_n \sim \text{Uniform}(0, 1)$ . Then, calculate the quantity

$$m = \sum_{i=1}^n \left\lfloor \frac{\log u_i}{\log(1-p)} \right\rfloor, \quad (C2)$$

where  $\lfloor \cdot \rfloor$  is the floor function, i.e.,  $\lfloor x \rfloor$  denotes the greatest integer less than or equal to  $x$ . The quantity  $N = n + m$  will then follow a negative binomial distribution with parameters  $n$  and  $p$ .

##### *Dirichlet*

The Dirichlet distribution is a multivariate generalization of the Beta distribution, and it is commonly used when modeling group proportions. Dirichlet random variables are constrained to be positive and sum to one. The Dirichlet distribution with argument  $\theta_1, \dots, \theta_k$  and parameters  $\alpha_1, \dots, \alpha_k$  is given by

$$p(\theta_1, \dots, \theta_k | \alpha_1, \dots, \alpha_k) = \frac{\Gamma(\alpha_1 + \dots + \alpha_k)}{\Gamma\alpha_1 \dots \Gamma\alpha_k} \prod_{i=1}^k \theta_i^{\alpha_i-1}, \quad \theta_1, \dots, \theta_k \geq 0, \quad \alpha_1, \dots, \alpha_k > 0, \quad \sum_{i=1}^k \theta_i = 1. \quad (C3)$$

To draw a random value  $\theta_1, \dots, \theta_k$  from a Dirichlet distribution with parameters  $\alpha_1, \dots, \alpha_k$ , first draw  $x_1, \dots, x_k$  independently from Gamma distributions with shape parameters  $\alpha_1, \dots, \alpha_k$  and common scale parameter equal to one. Then, set  $\theta_j = x_j / \sum_{i=1}^k x_i$ . The set of  $\theta$  will then follow a Dirichlet distribution.

### Multivariate Student- $t$ and Cauchy Distribution

The Student- $t$  distribution is often used as a robust alternative to the normal distribution because it is more heavily tailed than the normal distribution, and therefore reduces the effect of outliers on statistical analysis. A  $t$  distribution with  $\nu = 1$  degree of freedom is referred to as a Cauchy distribution, and it is functionally equivalent to a Lorentzian function. A  $p$ -dimensional multivariate  $t$  distribution with  $p$ -dimensional argument  $\mathbf{x}$ ,  $p$ -dimensional mean vector  $\mu$ ,  $p \times p$  scale matrix  $\Sigma$ , and degrees of freedom  $\nu$  is given by

$$p(\mathbf{x}|\mu, \Sigma, \nu) = \frac{\Gamma((\nu + p)/2)}{\Gamma(\nu/2)\nu^{p/2}\pi^{p/2}} |\Sigma|^{-1/2} \left[ 1 + \frac{1}{\nu} (\mathbf{x} - \mu)^T \Sigma^{-1} (\mathbf{x} - \mu) \right]^{-(\nu+p)/2}. \quad (\text{C4})$$

The 1-dimensional  $t$  distribution is obtained by replacing matrix and vector operations in Equation (C4) with scalar operations.

Although we do not simulate from a  $t$  distribution in this work, for completeness we include how to do so. To simulate a random vector  $\mathbf{t}$  from a multivariate  $t$  distribution with mean vector  $\mu$ , scale matrix  $\Sigma$ , and degrees of freedom  $\nu$ , first draw  $\mathbf{z}$  from a zero mean multivariate normal distribution with covariance matrix  $\Sigma$ . Then, draw  $x$  from a chi-square distribution with  $\nu$  degrees of freedom, and compute the quantity  $\mathbf{t} = \mu + \mathbf{z}\sqrt{\nu/x}$ . The quantity  $\mathbf{t}$  is then distributed according to the multivariate  $t$  distribution.

### Wishart and Inverse Wishart

The Wishart distribution describes the distribution of the  $p \times p$  sample covariance matrix, given the  $p \times p$  population covariance matrix, for data drawn from a multivariate normal distribution. Conversely, the inverse Wishart distribution describes the distribution of the population covariance matrix, given the sample covariance matrix, when the data are drawn from a multivariate normal distribution. The Wishart distribution can be thought of as a multivariate extension of the  $\chi^2$  distribution. A Wishart distribution with  $p \times p$  argument  $S$ ,  $p \times p$  scale matrix  $\Sigma$ , and degrees of freedom  $\nu$  is given by

$$p(S|\Sigma, \nu) = \left[ 2^{\nu p/2} \pi^{p(p-1)/4} \prod_{i=1}^p \Gamma\left(\frac{\nu + 1 - i}{2}\right) \right]^{-1} |\Sigma|^{-\nu/2} |S|^{(\nu-p-1)/2} \exp\left\{-\frac{1}{2} \text{tr}(\Sigma^{-1} S)\right\}, \quad (\text{C5})$$

where the matrices  $S$  and  $\Sigma$  are constrained to be positive definite. An inverse Wishart distribution with  $p \times p$  argument  $\Sigma$ ,  $p \times p$  scale matrix  $S$ , and degrees of freedom  $\nu$  is

$$p(\Sigma|S, \nu) = \left[ 2^{\nu p/2} \pi^{p(p-1)/4} \prod_{i=1}^p \Gamma\left(\frac{\nu + 1 - i}{2}\right) \right]^{-1} |S|^{\nu/2} |\Sigma|^{-(\nu+p+1)/2} \exp\left\{-\frac{1}{2} \text{tr}(\Sigma^{-1} S)\right\}, \quad (\text{C6})$$

where the matrices  $S$  and  $\Sigma$  are constrained to be positive definite.

To draw a  $p \times p$  random matrix from a Wishart distribution with scale matrix  $\Sigma$  and  $\nu$  degrees of freedom, first draw  $\mathbf{x}_1, \dots, \mathbf{x}_\nu$  from a zero mean multivariate normal distribution with  $p \times p$  covariance matrix  $\Sigma$ . Then, calculate the sum  $S = \sum_{i=1}^\nu \mathbf{x}_i \mathbf{x}_i^T$ . The quantity  $S$  is then a random draw from a Wishart distribution. Note that this technique only works when  $\nu \geq p$ . A random draw from the inverse Wishart distribution with scale matrix  $S$  and degrees of freedom  $\nu$  may be obtained by first obtaining a random draw  $W$  from a Wishart distribution with scale matrix  $S^{-1}$  and degrees of freedom  $\nu$ . The quantity  $\Sigma = W^{-1}$  will then follow an inverse Wishart distribution.

### REFERENCES

- Avni, Y., & Bahcall, J. N. 1980, ApJ, 235, 694  
 Babbedge, T. S. R., et al. 2006, MNRAS, 370, 1159  
 Barger, A. J., Cowie, L. L., Mushotzky, R. F., Yang, Y., Wang, W.-H., Steffen, A. T., & Capak, P. 2005, AJ, 129, 578  
 Blanton, M. R., et al. 2003, ApJ, 592, 819  
 Bower, R. G., Benson, A. J., Malbon, R., Helly, J. C., Frenk, C. S., Baugh, C. M., Cole, S., & Lacey, C. G. 2006, MNRAS, 370, 645  
 Brown, M. J. I., Dey, A., Jannuzi, B. T., Brand, K., Benson, A. J., Brodwin, M., Croton, D. J., & Eisenhardt, P. R. 2007, ApJ, 654, 858  
 Budavári, T., et al. 2005, ApJ, 619, L31  
 Cao, X., & Xu, Y.-D. 2007, MNRAS, 377, 425  
 Chib, S., & Greenberg, E. 1995, Amer. Stat., 49, 327  
 Cirasuolo, M., et al. 2007, MNRAS, 380, 585  
 Croom, S. M., Smith, R. J., Boyle, B. J., Shanks, T., Miller, L., Outram, P. J., & Loaring, N. S. 2004, MNRAS, 349, 1397  
 Croton, D. J., et al. 2005, MNRAS, 356, 1155  
 Dahlen, T., Mobasher, B., Somerville, R. S., Moustakas, L. A., Dickinson, M., Ferguson, H. C., & Giavalisco, M. 2005, ApJ, 631, 126  
 Davison, A. C., & Hinkley, D. V. 1997, Bootstrap Methods and their Application (Cambridge:Cambridge University Press)  
 Dellaportas, P., & Papageorgiou, I. 2006, Stat. Comput., 16, 57  
 Efron, B. 1987, J. Americ. Stat. Assoc., 82, 171  
 Efron, B., & Petrosian, V. 1992, ApJ, 399, 345  
 Faber, S. M., et al. 2007, ApJ, 665, 265  
 Fan, X., et al. 2001, AJ, 121, 54  
 Fan, X., et al. 2006, AJ, 131, 1203  
 Finlator, K., Davé, R., Papovich, C., & Hernquist, L. 2006, ApJ, 639, 672  
 Gelman, A., Carlin, J. B., Stern, H. S., & Rubin, D. B. 2004, Bayesian Data Analysis (2nd ed.; Boca Raton:Chapman & Hall/CRC)

- Gelman, A., Meng, X. L., & Stern, H. S. 1998, *Statistica Sinica*, 6, 733
- Gelman, A., Roberts, G., & Gilks, W. 1995, in *Bayesian Statistics 5*, ed. J. M. Bernardo, J. O. Berger, A. P. Dawid, & A. F. M. Smith (Oxford:Oxford University Press), 599
- Hao, L., et al. 2005, *AJ*, 129, 1795
- Harsono, D., & de Propriis, R. 2007, *MNRAS*, 380, 1036
- Hastings, W. K. 1970, *Biometrika*, 57, 97
- Ho, L. C. 2002, *ApJ*, 564, 120
- Hopkins, P. F., Hernquist, L., Cox, T. J., Di Matteo, T., Robertson, B., & Springel, V. 2006, *ApJS*, 163, 1
- Hopkins, P. F., Narayan, R., & Hernquist, L. 2006, *ApJ*, 643, 641
- Hopkins, P. F., Richards, G. T., & Hernquist, L. 2007, *ApJ*, 654, 731
- Hoyle, F., Rojas, R. R., Vogeley, M. S., & Brinkmann, J. 2005, *ApJ*, 620, 618
- Huynh, M. T., Frayer, D. T., Mobasher, B., Dickinson, M., Chary, R.-R., & Morrison, G. 2007, *ApJ*, 667, L9
- Jasra, A., Holmes, C.C., & Stephens, D.A. 2005, *Statistical Science*, 20, 50
- Jester, S. 2005, *ApJ*, 625, 667
- Jiang, L., et al. 2006, *AJ*, 131, 2788
- Kelly, B. C. 2007, *ApJ*, 665, 1489
- Kim, D.-W., et al. 2006, *ApJ*, 652, 1090
- La Franca, F., et al. 2005, *ApJ*, 635, 864
- Lauer, T. R., et al. 2007, *ApJ*, 662, 808
- Lin, Y.-T., & Mohr, J. J. 2007, *ApJS*, 170, 71
- Lynden-Bell, D. 1971, *MNRAS*, 155, 95
- Magorrian, J., et al. 1998, *AJ*, 115, 2285
- Maloney, A., & Petrosian, V. 1999, *ApJ*, 518, 32
- Marchesini, D., Celotti, A., & Ferrarese, L. 2004, *MNRAS*, 351, 733
- Marchesini, D., et al. 2007, *ApJ*, 656, 42
- Marchesini, D., & van Dokkum, P. G. 2007, *ApJ*, 663, L89
- Marconi, A., Risaliti, G., Gilli, R., Hunt, L. K., Maiolino, R., & Salvati, M. 2004, *MNRAS*, 351, 169
- Marshall, H. L., Tananbaum, H., Avni, Y., & Zamorani, G. 1983, *ApJ*, 269, 35
- Matute, I., La Franca, F., Pozzi, F., Gruppioni, C., Lari, C., & Zamorani, G. 2006, *A&A*, 451, 443
- Mauch, T., & Sadler, E. M. 2007, *MNRAS*, 375, 931
- Merloni, A. 2004, *MNRAS*, 353, 1035
- Metropolis, N., & Ulam, S. 1949, *J. Amer. Stat. Assoc.*, 44, 335
- Metropolis, N., Rosenbluth, A. W., Rosenbluth, M. N., Teller, A. H., & Teller, E. 1953, *J. Chem. Phys.*, 21, 1087
- Nakamura, O., Fukugita, M., Yasuda, N., Loveday, J., Brinkmann, J., Schneider, D. P., Shimasaku, K., & SubbaRao, M. 2003, *AJ*, 125, 1682
- Neal, R. M. 1996, *Statistics and Computing*, 6, 353
- Page, M. J., & Carrera, F. J. 2000, *MNRAS*, 311, 433
- Paltani, S., et al. 2007, *A&A*, 463, 873
- Press, W. H., & Schechter, P. 1974, *ApJ*, 187, 425
- Popesso, P., Biviano, A., Böhringer, H., & Romaniello, M. 2006, *A&A*, 445, 29
- Ptak, A., Mobasher, B., Hornschemeier, A., Bauer, F., & Norman, C. 2007, *ApJ*, 667, 826
- Richards, G. T., et al. 2006, *AJ*, 131, 2766
- Richardson, S., & Green, P. J. 1997, *J. Roy. Statist. Soc. Ser. B*, 59, 731
- Roeder, K., & Wasserman, L. 1997, *J. Amer. Stat. Assoc.*, 92, 894
- Rubin, D. B. 1981, *J. Educational Statistics*, 6, 377
- Rubin, D. B. 1984, *Annals of Statistics*, 12, 1151
- Scarlata, C., et al. 2007, *ApJS*, 172, 406
- Schafer, C. M. 2007, *ApJ*, 661, 703
- Schechter, P. 1976, *ApJ*, 203, 297
- Schneider, D. P., et al. 2005, *AJ*, 130, 367
- Soltan, A. 1982, *MNRAS*, 200, 115
- Spergel, D. N., et al. 2003, *ApJS*, 148, 175
- Steffen, A. T., Barger, A. J., Cowie, L. L., Mushotzky, R. F., & Yang, Y. 2003, *ApJ*, 596, L23
- Schmidt, M. 1968, *ApJ*, 151, 393
- Ueda, Y., Akiyama, M., Ohta, K., & Miyaji, T. 2003, *ApJ*, 598, 886
- Waddington, I., Dunlop, J. S., Peacock, J. A., & Windhorst, R. A. 2001, *MNRAS*, 328, 882
- Willott, C. J., Rawlings, S., Blundell, K. M., Lacy, M., & Eales, S. A. 2001, *MNRAS*, 322, 536
- Wolf, C., Wisotzki, L., Borch, A., Dye, S., Kleinheinrich, M., & Meisenheimer, K. 2003, *A&A*, 408, 499
- Wyithe, J. S. B., & Loeb, A. 2003, *ApJ*, 595, 614
- Yu, Q., & Tremaine, S. 2002, *MNRAS*, 335, 965